

The Milky Way in X-rays for an outside observer

Log(N)-Log(S) and Luminosity Function of X-ray binaries from RXTE/ASM data

H.-J. Grimm¹, M. Gilfanov^{1,2}, and R. Sunyaev^{1,2}

¹ Max-Planck-Institut für Astrophysik, Garching, Germany

² Space Research Institute, Moscow, Russia

Received 18-09-01 / Accepted 03-06-02

Abstract. We study the Log(N)–Log(S) and X-ray luminosity function in the 2–10 keV energy band, and the spatial (3-D) distribution of bright, $L_X \geq 10^{34} - 10^{35}$ erg s^{−1}, X-ray binaries in the Milky Way. In agreement with theoretical expectations and earlier results we found significant differences between the spatial distributions of low (LMXB) and high (HMXB) mass X-ray binaries. The volume density of LMXB sources peaks strongly at the Galactic Bulge whereas HMXBs tend to avoid the inner $\sim 3 - 4$ kpc of the Galaxy. In addition HMXBs are more concentrated towards the Galactic Plane (scale heights of ≈ 150 and ≈ 410 pc for HMXB and LMXB correspondingly) and show clear signatures of the spiral structure in their spatial distribution. The Log(N)–Log(S) distributions and the X-ray luminosity functions are also noticeably different. LMXB sources have a flatter Log(N)–Log(S) distribution and luminosity function. The integrated 2–10 keV luminosities of all X-ray binaries in the Galaxy, *averaged* over 1996–2000, are $\sim 2 - 3 \cdot 10^{39}$ (LMXB) and $\sim 2 - 3 \cdot 10^{38}$ (HMXB) erg s^{−1}. Normalised to the stellar mass and the star formation rate, respectively, these correspond to $\sim 5 \cdot 10^{28}$ erg s^{−1} M_⊙^{−1} for LMXBs and $\sim 5 \cdot 10^{37}$ erg s^{−1}/(M_⊙ yr^{−1}) for HMXBs. Due to the shallow slopes of the luminosity functions the integrated emission of X-ray binaries is dominated by the ~ 5 –10 most luminous sources which determine the appearance of the Milky Way in the standard X-ray band for an outside observer. In particular variability of individual sources or an outburst of a bright transient source can increase the integrated luminosity of the Milky Way by as much as a factor of ~ 2 . Although the average LMXB luminosity function shows a break near the Eddington luminosity for a 1.4 M_⊙ neutron star, at least 12 sources showed episodes of super-Eddington luminosity during ASM observations. We provide the maps of distribution of X-ray binaries in the Milky Way in various projections, which can be compared to images of nearby galaxies taken by CHANDRA and XMM-Newton.

Key words. X-rays: binaries – X-rays: galaxies – Galaxy: general – Galaxy: structure – Galaxies: spiral – Stars: luminosity function

1. Introduction

Recently the CHANDRA X-ray observatory studied the distributions and luminosity functions of X-ray binaries in at least 7 spiral, e.g. M 81 (Tennant et al. 2001), 2 elliptical, e.g. NGC 4697 (Sarazin et al. 2000), and 2 starburst galaxies, M 82 (Zezas et al. 2001) and Antennae (Fabbiano et al. 2001). The main discovery of these CHANDRA observations was the existence of numerous point-like sources with luminosities in the CHANDRA spectral band considerably higher than the Eddington luminosity of a 1.4 M_⊙ neutron star. Nearby galaxies observed by CHANDRA

have a great advantage compared to observations of X-ray sources in our Galaxy: All objects observed in a particular galaxy are equidistant and therefore it is straightforward to construct the luminosity function in the CHANDRA band. However, even with the angular resolution and sensitivity of CHANDRA we are restricted to nearby galaxies ($d \lesssim 50$ Mpc) and we are able to observe only the high luminosity end of the luminosity function.

Observations of compact sources inside our Galaxy thus open the unique possibility to construct a luminosity function in a much broader range of luminosities and this might be important to construct the synthesised spectrum of the LMXB and HMXB populations of the Galaxy in a broad spectral range from 0.1–500 keV using data from all existing spacecraft.

Send offprint requests to: Hans-Jakob Grimm, e-mail: grimm@mpa-garching.mpg.de

Correspondence to: Max-Planck-Institut für Astrophysik, Karl-Schwarzschild-Str. 1, 85748 Garching, Germany

In this paper we use data of the All-Sky Monitor (ASM) (Levine et al. 1996) aboard the Rossi X-ray Timing Explorer (Brandt et al. 1996) to investigate the following topics.

- Using ASM data, existing information about the source distances and a model of the mass distribution in the Milky Way we constructed the luminosity function of high and low mass X-ray binaries in our Galaxy.
- Distribution and number of high mass X-ray binaries are expected to trace the location and reflect the rate of star formation. The X-ray luminosity of starburst galaxies might become an additional source of information about the star formation rate in these galaxies. Moreover knowledge of the luminosity of HMXBs versus star formation rate opens the way to find the volume emissivity of our universe at different redshifts in hard X-rays due to starburst and young galaxies.
- The luminosity of the LMXB component is proportional to the total mass of the old stellar population of the Milky Way. Concerning the volume emissivity of galaxies these data will provide information about the contribution of elliptical galaxies and old star populations in spiral galaxies only at sufficiently low redshifts ($z < 0.4 - 0.5$). To obtain the volume emissivity due to old star populations at higher redshift we need to know a model of the mass exchange rate evolution.
- Our Galaxy should become an important point in the future calibration curves of L_{HMXB}/SFR and $L_{\text{LMXB}}/M_{\text{galaxy}}$.
- Our analysis of ASM data permits us to show how our Galaxy would look from outside in different projections. This will allow us to compare data about our Galaxy with new CHANDRA observations.
- Surprisingly enough, just the comparatively few most luminous Galactic X-ray binaries practically dominate the X-ray luminosity of our Galaxy. The majority of the brightest X-ray binaries are extremely variable on all time scales from milliseconds to years–tens of years. Therefore the luminosity of our Galaxy as a whole would also be subject to strong variability. This is important because with a powerful X-ray telescope such as XEUS it will be possible to detect X-ray flux from distant galaxies on the level of $L \sim 10^{40} \text{ erg s}^{-1}$ but only short time scale variability would permit to distinguish the collective emission of X-ray binaries from the low luminosity, AGN-type activity of the nucleus. Black holes are unable to produce strong variability with characteristic times significantly shorter than a few $0.01 \text{ s } \frac{M_{\text{BH}}}{M_{\odot}}$ (Sunyaev & Revnivtsev 2000). For super-massive black holes the characteristic time is of order or above $\sim 10^3 \text{ s}$.
- Our analysis of ASM data and data from other spacecraft shows that at least for 17 X-ray sources in our Galaxy ASM or other spacecraft detected flux reaching or exceeding the level corresponding to the Eddington critical luminosity for a $1.4 M_{\odot}$ neutron star, see Table 1. Maximal fluxes detected were up to 10 times higher

than the Eddington value for a neutron star. In at least 7 sources the compact object has been identified as a neutron star based on the detection of X-ray pulsations or X-ray bursts, therefore we know with certainty that the peak luminosity exceeded the Eddington limit. Moreover, the total number of super-Eddington sources might be higher because we know from the broad band observations that the bulk of the luminosity can be emitted outside the ASM sensitivity band.

In terms of the spatial distribution of X-ray binaries this paper elaborates on works done earlier that also distinguished between low and high mass systems but used substantially smaller samples.

Previously White et al. (1980), Lamb et al. (1980), Nagase (1989) and Verbunt (1996) noted the correlation of the positions of accreting X-ray pulsars with high mass companions with the location of spiral arm features of the Milky Way. Based on a larger sample of HMXBs with measured distances we show that indeed the spatial distribution of HMXBs follows the spiral structure of the Galaxy.

Using distance estimates and angular distribution of LMXBs van Paradijs & White (1995) and White & van Paradijs (1996) investigated the spatial distribution of LMXBs and BHC in our Galaxy, particularly in the Galactic disk. They estimated values for the vertical (290 pc and 710 pc for BHC and NS binaries) and radial scales (4.5 kpc for NS binaries) of the disk. These values are in general agreement with those obtained in this paper, that are based on a considerably larger number of sources. Grebenev et al. (1996) found good agreement between the source distribution observed by ART-P/GRANAT in the Galactic Centre region and the stellar mass distribution in the Galactic Bulge. We thus have a reasonably good knowledge about the distribution of LMXBs in the Galaxy.

2. RXTE All-Sky Monitor Data

In order to construct the Log(N)–Log(S) distributions and luminosity functions we used the publicly available data of ASM. The ASM instrument is sensitive in the 2-10 keV energy band which is divided into 3 broad energy channels and provides 80% sky coverage for every satellite orbit (~ 90 minutes). Due to its all-sky nature and long operational time, ~ 5 years, the ASM instrument is ideally suited for studying time averaged properties of sources. The light curves are obtained by RXTE GOF (Levine et al. 1996) for a preselected set of sources from the ASM catalogue. The catalogue consists of sources which have reached an intensity of more than 5 mCrab at any time (Lochner & Remillard 1997), and as of June 2000 included 340 sources of which 217 are galactic and 112 extragalactic, and 10 unidentified. The distribution of galactic sources on the sky is shown in Fig. 1. For a detailed description of selection criteria and a list of sources see Lochner & Remillard

Table 1. Persistent, transient and extragalactic X-ray binaries for which episodes of near- or super-Eddington flux were detected. The maximum luminosities from ASM observations refer to the dwell-time light curves (90 s observations every 90 minutes). Thus the values might differ from the luminosities given in Tables 5 and 6.

Source	type	M ₁ [M _⊙]	Luminosity [10 ³⁸ erg s ⁻¹] average ^(a) peak		Energy range [keV]	Ref. ^(b)	distance [kpc]	Ref. ^(c)
Persistent sources								
Cir X-1	LMXB	NS	4.4	12	2–10	(1)	10.9	(i)
GRS 1915+105	LMXB	14-30	3.7	15	2–10	(1)	12.5	(ii)
Sco X-1	LMXB	NS	2.7	9.4	2–10	(1)	2.8	(iii)
Cyg X-2	LMXB	NS	1.8	4.2	2–10	(1)	11.3	(i),(iv),(v),(vi),(vii)
GX 349+2	LMXB	NS	1.6	3.2	2–10	(1)	9.2	(i),(vii),(viii)
GX 17+2	LMXB	NS	1.5	3.0	2–10	(1)	9.5	(i),(vii),(ix),(x)
GX 5-1	LMXB	NS	1.4	2.2	2–10	(1)	7.2	(i),(vii)
GX 340+0	LMXB	NS	1.3	2.2	2–10	(1)	11.0	(i),(vii)
Cyg X-3	HMXB	NS(?)	0.5	2.1	2–10	(1)	9.0	(xi)
X 1624-490	LMXB	NS	0.24	3.3	2–10	(1)	13.5	(ix)
GRO J1744-28	LMXB	NS	0.15	4	8–20	(2)	8.5	(xii)
Transient sources								
V4641 Sgr	HMXB	9.6	33		2–10	(1)	9.9	(xiii)
GS 2023+338	LMXB	12	11		1–40	(3)	4.3	(xiv)
4U 1608-52	LMXB	NS	9.2		2–20	(4)	4.0	(i),(x),(xv)
N Musc 91	LMXB	7	6.1		1–6	(5)	5.5	(xvi),(xvii),(xviii)
XTE J1550-564	LMXB	10.5	5.3		2–10	(1)	5.3	(xix)
N Oph 77	LMXB	5	5.4		2–18	(6)	7.0	(xviii),(xx)
GS 2000+251	LMXB	6	2.2		1–6	(7)	2.7	(xviii),(xxi)
Magellanic Clouds sources								
SMC X-1	HMXB	NS	2.0	17	2–10	(1)	60 ^(d)	
LMC X-1	HMXB	4.7√cos <i>i</i>	1.5	13	2–10	(1)	50 ^(d)	
LMC X-2	LMXB	NS	1.5	17	2–10	(1)	50 ^(d)	
LMC X-3	HMXB	> 5.8	1.5	17	2–10	(1)	50 ^(d)	
LMC X-4	HMXB	NS	0.38	15	2–10	(1)	50 ^(d)	

^(a) average luminosity observed by ASM.

^(b) Reference for the peak luminosity.

(1) ASM (this paper), (2) Sazonov et al. (1997), (3) Tanaka (1992), (4) Nakamura et al. (1989), (5) Kitamoto et al. (1992), (6) Watson et al. (1978), (7) Tsunemi et al. (1989).

^(c) Reference(s) for the distance: (i) van Paradijs & White (1995), (ii) Mirabel & Rodriguez (1994), (iii) Bradshaw et al. (1999), (iv) Orosz & Kuulkers (1999), (v) Cowley et al. (1979), (vi) Smale (1998), (vii) Penninx (1989), (viii) Wachter & Margon (1996), (ix) Christian & Swank (1997), (x) Ebisuzaki et al. (1984), (xi) Predehl et al. (2000), (xii) Nishiuchi et al. (1999), (xiii) Orosz et al. (2000), (xiv) King (1993), (xv) Nakamura et al. (1989), (xvi) Greiner et al. (1994), (xvii) Orosz et al. (1996), (xviii) Barret et al. (1996), (xix) Orosz et al. (2002), (xx) Martin et al. (1995), (xxi) Chevalier & Ilovaisky (1990)

^(d) assuming a distance of 50 kpc for LMC and 60 kpc for SMC.

(1997). The 1 day sensitivity of ASM is ≈ 10 mCrab corresponding to a count rate of 0.75 cnts s^{-1} . The ASM count rate has been converted to energy flux assuming a Crab-like spectrum and using the observed Crab count rate:

$$F[\text{erg s}^{-1} \text{ cm}^{-2}] = 3.2 \cdot 10^{-10} \cdot R[\text{cnts s}^{-1}]. \quad (1)$$

The 1-dwell ASM light curves have been retrieved from the RXTE public archive¹ at HEASARC and cover a time period from the start of the mission through 27/04/00. In order to construct Log(N)–Log(S) the light curves have been averaged over the entire period of available data which might differ for different sources. We did not account in any way for orbital variations or eclipses, as e.g. in Cen X-3.

¹ ftp://legacy.gsfc.nasa.gov/xte/data/archive/ASMPProducts/definitive_1dwell/

Important for the analysis presented below are the questions of systematic errors in the light curves and of the completeness limit of the ASM catalogue.

2.1. Systematic errors

The ASM light curves are assumed to have a systematic error at the level of $\sim 3\%$ which is added in quadrature to the statistical errors in the light curves provided by the RXTE GOF. The systematic error has been estimated using Crab data and refers to the \sim dwell–day time scales. The formal errors for the average fluxes calculated from the entire ASM light curves are very small $\sim 0.1 - 0.2$ mCrab ($\sim 1 - 2 \cdot 10^{-2} \text{ cnts s}^{-1}$). In the presence of systematic errors this might not correctly characterise the accuracy of the average flux estimate, especially for weak

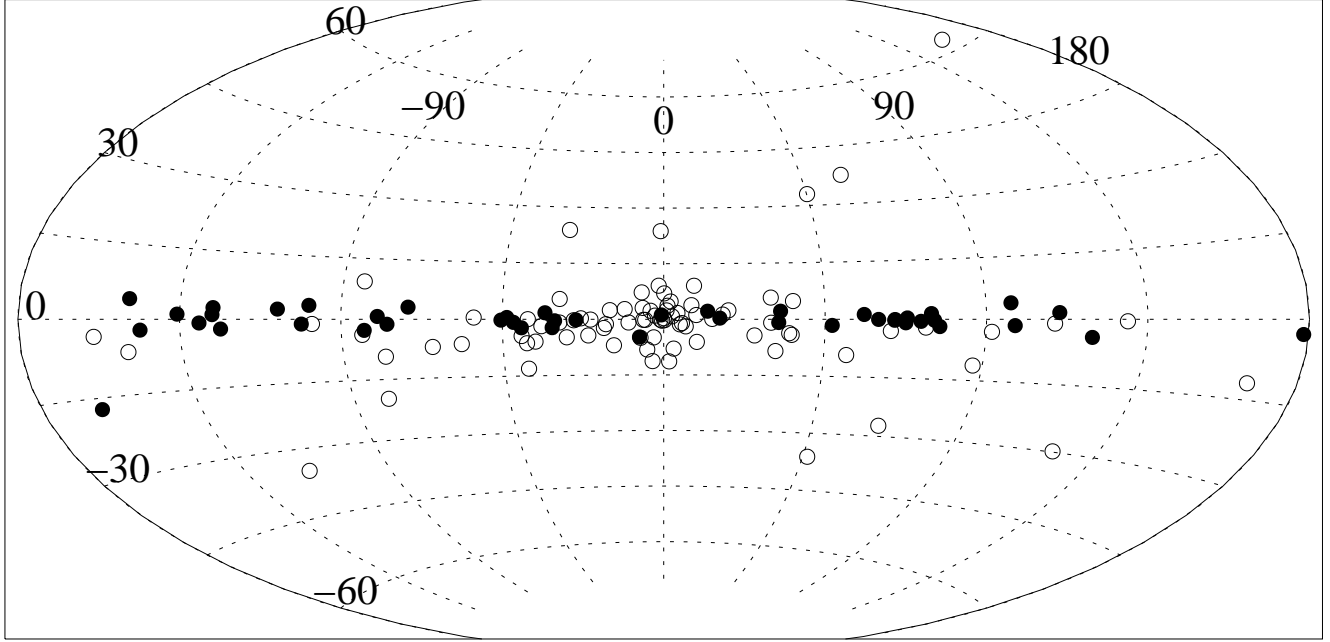


Fig. 1. Distribution of LMXBs (open circles) and HMXBs (filled circles) in the Galaxy. In total 86 LMXBs and 52 HMXBs are shown. Note the significant concentration of HMXBs towards the Galactic Plane and the clustering of LMXBs in the Galactic Bulge.

Table 2. List of the sources used to estimate systematic errors.

Source	average flux ^(a) [cnts s ⁻¹]	excess RMS ^(b) [cnts s ⁻¹]
Cas A	4.9 ± 0.007	~ 0.08
Tycho SNR	1.3 ± 0.007	~ 0.04
Puppis A	0.84 ± 0.008	~ 0.05
Vela pulsar	0.75 ± 0.008	~ 0.01
CTB 33	0.35 ± 0.014	~ 0.07
PSR 1259-63	0.18 ± 0.012	~ 0.01
NGC 2024	0.09 ± 0.008	~ 0.02
PSR J1713+0747	0.07 ± 0.015	~ 0.01
PSR 1957+20	0.06 ± 0.012	~ 0.02
XTE J1906+090	0.04 ± 0.011	~ 0.03

^(a)the errors are formally calculated using the errors in the light curves.

^(b)upper limit on the unaccounted contribution of the systematic errors to the averaged flux, estimated from Fig. 2.

sources. The contribution of systematic errors to the average flux estimate depends on their statistical properties, in particular their correlation time scale. In order to investigate these properties we selected several sources believed to have constant X-ray flux, like SNRs or rotation powered pulsars, see Table 2, and rebinned their light curves with different bin durations ranging from 1 to 200 days. For each binned light curve we computed the expected RMS from the errors given with the light curves and compared it with the observed RMS. The results are shown

in Fig. 2. Ideally there should be a one-to-one correspondence between expected and observed RMS (straight line in Fig. 2). As can be seen from Fig. 2 this is not the case. The observed RMS somewhat exceeds the expected value, the discrepancy increasing towards large bin durations (~ 50 -200 days). The excess variance at large bin durations (lower-left part in Fig. 2) gives an upper limit on the unaccounted systematic error in the averaged flux estimate. As can be seen from Fig. 2 the particular value of the systematic error, though varying from source to source, is in the range of 0.01 – 0.1 cnts s⁻¹. We assumed a value of 0.05 cnts s⁻¹ (to be added in quadrature to the statistical error). We further verified that our conclusions are not sensitive to the value of the systematic error.

For 15 sources we obtain statistically significant, $\geq 3\sigma$, negative average count rates. The majority of these sources, namely 14, are located in the Small and Large Magellanic Cloud and their negative average flux is apparently caused by source interference in these crowded regions. The remaining source also appears to suffer from interference with nearby sources. In particular, we have noticed that some of the light curves show a clear drop below zero count rate coincident in time with addition of new sources located nearby to the ASM catalogue. All these sources are excluded from our analysis.

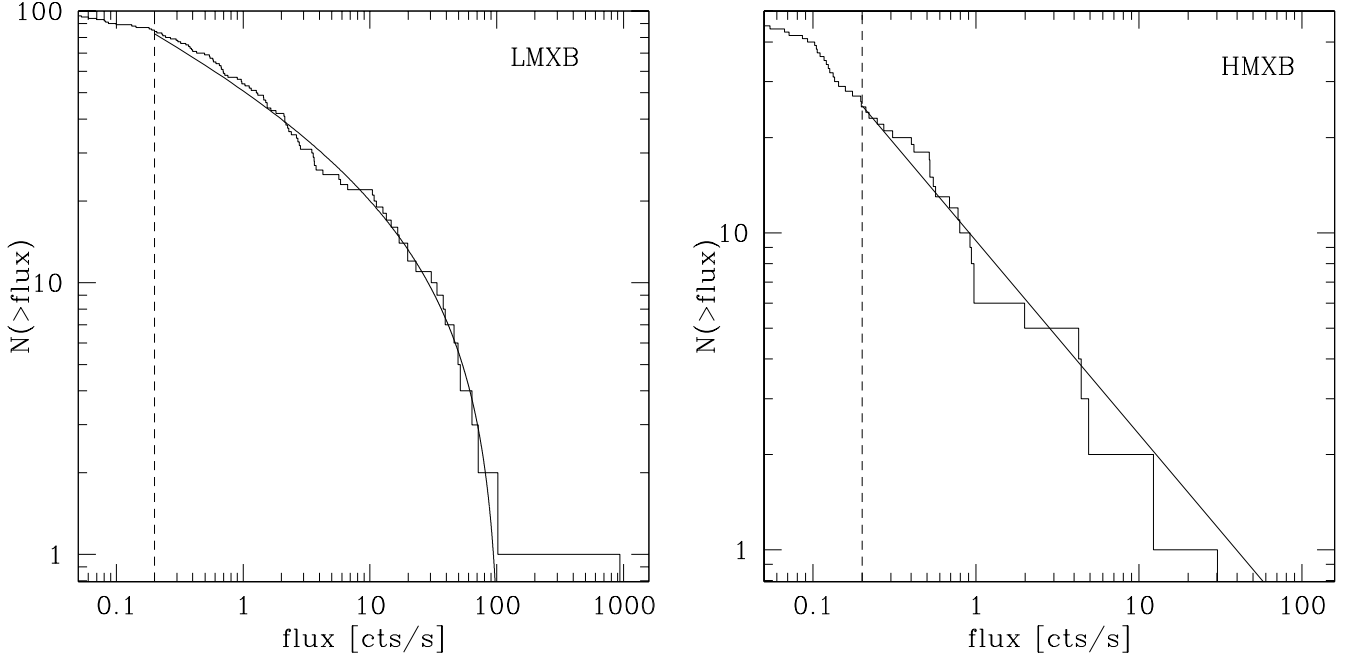


Fig. 5. Number–flux relation for galactic X-ray binaries. The vertical dashed line corresponds to our completeness limit of 0.2 cts s^{-1} . The solid lines are the best fit models to the ASM data – a power law for HMXBs and a power law with cutoff in the differential $\text{Log}(N)$ – $\text{Log}(S)$ distributions at 110 cts s^{-1} for LMXBs (see Eqs.(2) and (3)).

Table 3. The best fit values for the number–flux relation for different classes of galactic sources from the ASM catalogue.

Subsample	no. of sources ⁽¹⁾ /all sources	cutoff [cts s^{-1}]	normalisation	slope	quality of fit (K-S test)
all galactic	131/217 ⁽²⁾	110	88	0.34 ± 0.05	92%
	132/217	–	72	0.41 ± 0.04	51%
LMXB	83/105 ⁽²⁾	110	83	0.2 ± 0.06	71%
	84/105	–	56	0.3 ± 0.05	0.5%
HMXB	25/51	–	9.4	$0.61^{+0.14}_{-0.12}$	46%
SNR	6/7	–	4.8	$0.36^{+0.22}_{-0.19}$	98%
CV	5/10	–	0.5	1.68 ± 0.61	98%

⁽¹⁾ Number of sources above the completeness limit of 0.2 cts s^{-1} .

⁽²⁾ For fits with a cutoff the brightest source, Sco X-1, was excluded.

2.2. Completeness

Important for the analysis presented below are two aspects of completeness:

1. completeness flux limit of the ASM sample of the X-ray sources
2. completeness of the sample of galactic X-ray binaries which are optically identified and for which distance measurements are available

The first problem arises for example in studying $\text{Log}(N)$ – $\text{Log}(S)$ distribution of all galactic sources and is addressed below. The second problem is important in analysing $\text{Log}(N)$ – $\text{Log}(S)$ distributions of various types of galactic X-ray sources and especially their luminosity functions. It is discussed in Sect. 4.

Due to the present method of construction of the ASM catalogue its completeness limit is difficult to assess in any

straightforward way. By definition the ASM sample includes all sources, galactic and extragalactic, which have reached an intensity of 5 mCrab at any time, which corresponds to a completeness limit of $\sim 0.37 \text{ cts s}^{-1}$. On the other hand we know from the same ASM light curves that non-transient Galactic X-ray binaries have typical values of the ratio of maximum flux (on the time scale of dwell \sim day) to average flux of the order of few. Therefore, in terms of long term average values the ASM catalogue might be complete down to lower fluxes.

In order to indirectly probe the completeness limit of the ASM sample we use the fact that the $\text{Log}(N)$ – $\text{Log}(S)$ relation for extragalactic sources is well known and follows a power law with index $-3/2$ (Forman et al. 1978), down to $\sim 3.8 \cdot 10^{-14} \text{ erg s}^{-1} \text{ cm}^{-2}$ (Ogasaka et al. 1998) which corresponds to ASM count rate of $1.2 \cdot 10^{-4} \text{ cts s}^{-1}$. The $\text{Log}(N)$ – $\text{Log}(S)$ relation for extragalactic sources

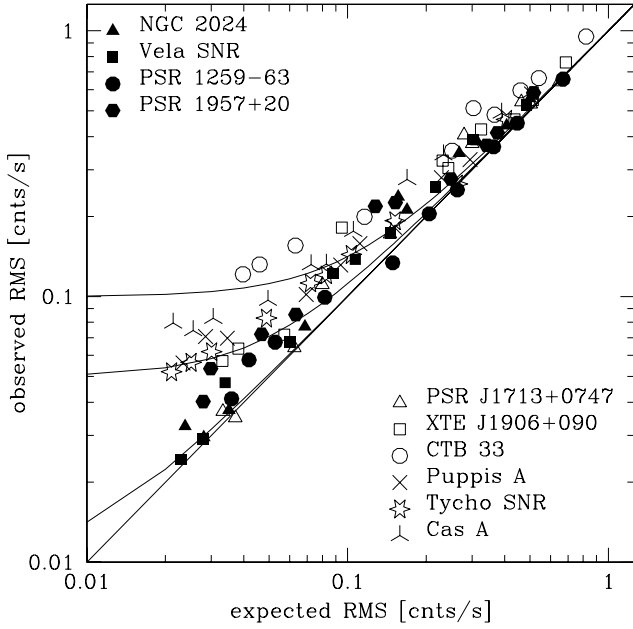


Fig. 2. Observed versus expected RMS for 10 different sources and for different time binnings. The bin duration varies from dwell time scale, i.e. ~ 90 seconds (upper right corner), to 200 days (lower left corner). Although there is considerable spread, the observed RMS is generally higher than expected, especially at large bin durations exceeding 50 days (expected RMS < 0.1 cnts s^{-1}). Assuming that systematic and statistical errors are independent the systematic error may be added to the statistical error in quadrature. This is shown by the solid curves for three different values of the systematic error: 0.01, 0.05 and 0.1 cnts s^{-1} .

based on ASM data is compared with HEAO A-1 and ASCA results in Fig. 3. One can see that flattening of the source counts caused by incompleteness of the sample begins at a count rate of ~ 0.1 cnts s^{-1} .

Therefore we set, somewhat arbitrarily, the completeness limit of the ASM sample of the X-ray sources at 0.2 cnts s^{-1} . We verified that our conclusions are not sensitive to the exact value.

3. The Log(N)–Log(S) distributions

In order to calculate the number–flux relations the ASM light curves were averaged over the entire time span of available data for each source. The resulting Log(N)–Log(S) relation for galactic sources is shown in Fig. 4. The differentiation between galactic and extragalactic sources was done using SIMBAD database. The overall shape and normalisation of the Log(N)–Log(S) relation of Galactic sources is similar to that obtained by UHURU (Forman et al. 1978) and ARIEL V (Warwick et al. 1981). The UHURU result (Matilsky et al. 1973) is schematically shown in Fig. 4 by the solid line. The Log(N)–Log(S) re-

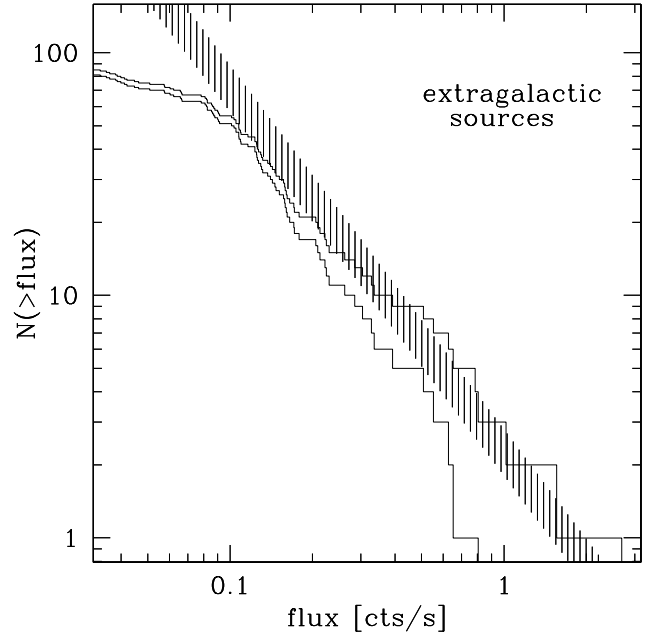


Fig. 3. Log(N)–Log(S) distribution of extragalactic sources. Magellanic Cloud sources have been omitted. The upper histogram contains all extragalactic sources, the lower histogram excludes 4 nearby galaxy clusters (Perseus, Virgo/M 87, Coma and Centaurus). The shaded region shows the Log(N)–Log(S) obtained by HEAO-1 A-2 for high latitude ($|b| > 20^\circ$) sources (Piccinotti et al. 1982). The width of the shaded region roughly accounts for the uncertainty of the RXTE/ASM and HEAO-1 A-2 calibration.

lation for different types of Galactic sources is also shown in Fig. 4.

We further selected X-ray binaries from the sample and divided them into low mass (LMXB) and high mass (HMXB) binaries according to the mass of the optical companion, using the mass of the secondary, M_2 , of $2.5 M_\odot$ to separate high and low mass systems. The precise value of this boundary affects classification of only few X-ray binaries (Her X-1, GX 1+4, GRO J1655-40 etc.). In doing so we used SIMBAD database, the Catalogue of X-ray Binaries (van Paradijs 1994), the Catalogue of CV, LMXB and related objects (Ritter & Kolb 1998), the catalogues of low-mass X-ray binaries (Liu et al. 2001) and high-mass X-ray binaries (Liu et al. 2000) and in some cases publications on individual sources. Recently the donor star in GRS 1915+105 was identified to be a K or M giant (Greiner et al. 2001) so this source is classified as an LMXB. Of 115 galactic X-ray binaries with average ASM flux exceeding our completeness limit of 0.2 cnts s^{-1} only 6 sources were left unclassified. The fraction of unclassified sources is $\sim 5\%$ and they have fluxes in the $3 \cdot 10^{-13}$ to 10^{-11} cnts s^{-1} range and therefore should not affect our conclusions in any significant way. The compilation of galactic X-ray binaries with type, optical companion, average flux and, if available, distance

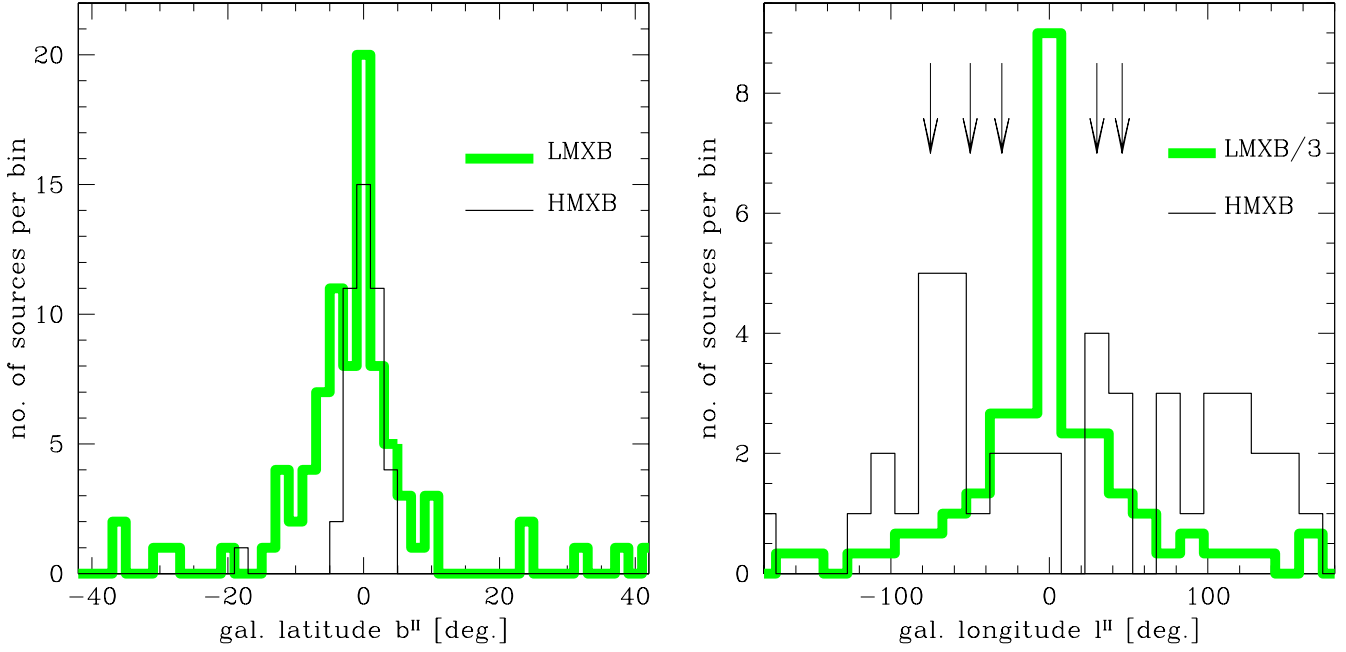


Fig. 6. The distribution of Galactic HMXBs (solid lines) and LMXBs (thick grey lines) against Galactic latitude b^{II} (left panel) and longitude l^{II} (right panel). The distribution against b^{II} of HMXBs shows a stronger concentration towards the Galactic plane compared to LMXBs. Along l^{II} LMXBs show a strong concentration in the direction towards the Galactic centre. The arrows in the right panel mark the positions of the tangential points of spiral arms. The broad hump in the HMXB distribution at $l^{II} = 100^\circ - 160^\circ$ is mostly composed of relatively low luminosity sources in the Perseus and Cygnus arms. Note that on the right panel the number of LMXBs is divided by 3.

and average luminosity is available in electronic form at <http://www.mpa-garching.mpg.de/~grimm/>. The resulting Log(N)–Log(S) relations for LMXBs and HMXBs are shown in Fig. 5.

To fit the observed Log(N)–Log(S) distributions we used the usual power law in the form:

$$N(> S) = k \cdot S^{-a} \quad (2)$$

where $N(> S)$ is the number of sources with fluxes higher than S , a is the slope, and k the normalisation. S is measured in ASM cts s $^{-1}$. In order to calculate the best fit values of the parameters we use a Maximum-Likelihood method in the form suggested by Murdoch & Crawford (1973). This implementation of the M-L method takes into account the errors associated with the flux. Since the systematic error dominates the averaged flux error we used the value of 0.05 cts s $^{-1}$ from Sect. 2.1 as an estimate of the error. The error is assumed to be Gaussian. Only sources with an averaged flux above 0.2 cts s $^{-1}$ were used in the fit. The best fit values for different types of Galactic sources are given in Table 3. The errors given are an estimate of the 1σ errors for one parameter of interest derived from the Maximum-Likelihood method. In order to characterise the quality of the fit we used the Kolmogorov-Smirnov test.

As is obvious from Fig. 5 and the results of the K-S test (Table 3) a simple power law distribution does not describe the observed Log(N)–Log(S) relation for LMXBs. A

gradual steepening of the Log(N)–Log(S) relation occurs towards higher fluxes. Similar behaviour was also found by UHURU (Matlisky et al. 1973) and OSO-7 (Markert et al. 1979). We therefore modified the simple power law in the form:

$$N(> S) = k \cdot (S^{-a} - S_{max}^{-a}) \quad (3)$$

This corresponds to a cutoff in the differential Log(N)–Log(S) relation at flux $S = S_{max}$. The value of the cutoff was chosen to $S_{max} = 110$ cts s $^{-1}$. The results, however, are not very sensitive to the actual value of S_{max} . The above value of S_{max} corresponds to the ASM flux from a 1.4 M $_{\odot}$ neutron star located at a distance of 6.5 kpc (average distance of LMXBs from the Sun) and radiating at Eddington luminosity. For fitting the Log(N)–Log(S) of all galactic and LMXB sources with cutoff we excluded the brightest source, Sco X-1, from the sample since its flux is far higher than the cutoff. As can be seen from Table 3 and Fig. 5 introduction of the cutoff significantly improves the quality of the fit for LMXBs. On the other hand it does not change significantly the results for other types of Galactic sources, especially HMXBs. Note that the steepening of the Log(N)–Log(S) for LMXBs is not an artifact of the incompleteness of the source sample at low fluxes. The numbers do not change qualitatively if we increase the low flux limit by a factor of 2 – the values of K-S probability are 6% and 68% for a single power law and a power law with cutoff in the form of Eq. (3), respectively.

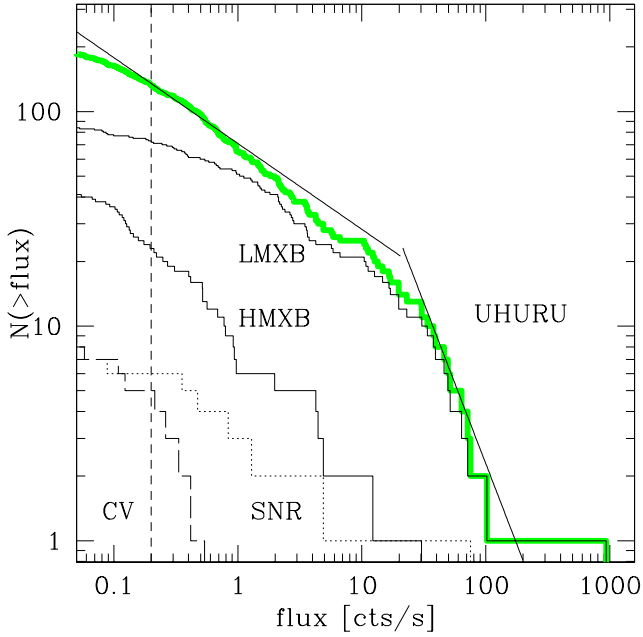


Fig. 4. Number–flux relation for all galactic sources derived from the entire ASM sample. The broken solid line shows schematically the number–flux relation for the low–latitude $|b| < 20^\circ$ sources obtained by UHURU (Matilsky et al. 1973). The vertical dashed line shows approximate completeness limit of the ASM sample. The thick grey histogram shows the $\text{Log}(N)$ – $\text{Log}(S)$ for all Galactic sources observed by ASM. The four lower histograms show the contributions of different classes of sources to the total galactic $\text{Log}(N)$ – $\text{Log}(S)$.

4. Spatial distribution of X-ray binaries

Progress in the number of distance determinations and identifications of secondary stars in X-ray binaries in the last decade opens the opportunity to study the 3-D distribution of XRBs in more detail than was previously possible. Notwithstanding the still relatively small number of X-ray sources and the sometimes poor accuracy of distance determinations it is now possible to compare the observed distribution of XRBs with theoretical expectations. This is not only interesting in itself but, because of the flux limited nature of the ASM sample, knowledge of the spatial distribution is required in order to derive the luminosity function. Due to the above mentioned uncertainties and the flux limitation of the sample it is still not possible to unambiguously determine shape and parameters of the XRB distribution. We therefore adopted an approach in which we use the standard model of the stellar mass distribution in the Galaxy as a starting point and adjust, whenever possible, its parameters to fit observed distributions of low and high mass X-ray binaries. As the luminosity function depends somewhat on the assumed spatial distribution, we verify that variations of the parameters, which can not be determined from the data do not affect derived luminosity functions significantly.

Table 4. The parameters of the standard Galaxy model.

parameter	meaning	value	
		HMXB	LMXB
q	oblateness of bulge	–	0.6
γ	–	–	1.8
R_e	scale length of spheroid	–	2.8 kpc
b	–	–	7.669
r_0	scale length of bulge	–	1 kpc
r_t	truncation radius of bulge	–	1.9 kpc
r_d	scale length of disk	3.5 kpc	3.5 kpc
r_z	vertical scale of disk	150 pc	410 pc
r_m	inner disk cut-off	6.5 kpc	6.5 kpc
R_{mass}	mass ratios	1:0:0	2:1:0.8
	Disk:Bulge:Spheroid		

4.1. Angular distribution of X-ray binaries

The all-sky map shown in Fig. 1 demonstrates vividly that the angular distributions of high and low mass X-ray binaries over the sky differ significantly. This fact is further illustrated by the angular distributions against Galactic latitude and longitude shown in Fig. 6. The figures illustrate the well-known fact that HMXBs are strongly concentrated towards the Galactic plane. In addition drastic difference in the longitude distributions of HMXBs and LMXBs can be noticed, with the latter significantly concentrated towards the Galactic Centre/Bulge and the former distributed in clumps approximately coinciding with the location of tangential points of the spiral arms, see e.g. Englmaier & Gerhard (1999); Simonson (1976).

4.2. Source distances and 3-D distribution of X-ray binaries

In order to study the *spatial* distribution of X-ray binaries we collected source distances from the literature. We found distances for 140 X-ray binaries from the ASM sample. For X-ray binaries with an average flux above the ASM completeness limit, used for constructing the luminosity functions in Sect. 5, distances were determined for all but 8 sources. In cases when the published distance estimates disagree significantly we used the least model dependent estimates or their average. For the compilation of the source distances see <http://www.mpa-garching.mpg.de/~grimm/>. The spatial distribution of X-ray binaries in various projections is shown in Fig. 7–9.

4.3. The Galaxy model

As a starting point in constructing the spatial distribution of X-ray binaries we employ the standard three component model of the stellar mass distribution in the Galaxy (Bahcall & Soneira 1980), consisting of bulge, disk and spheroid. The parameterisation of bulge and disk is taken from Dehnen & Binney (1998) and for the spheroid we

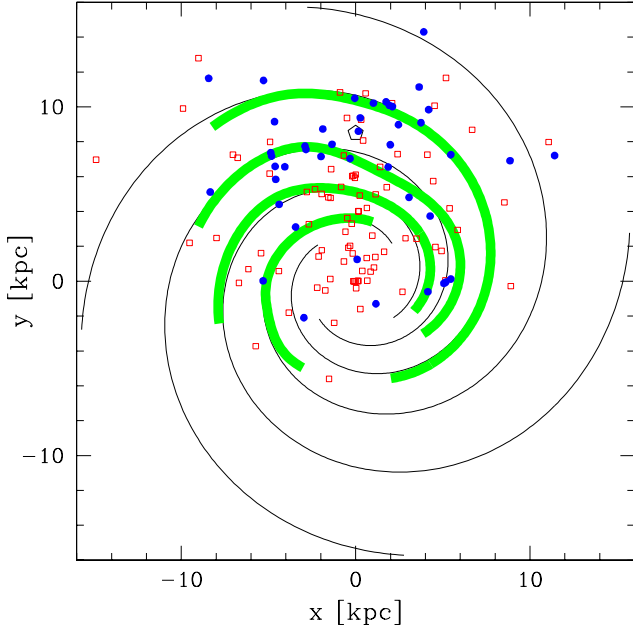


Fig. 7. Face-on view of the Galaxy – distribution of low mass (open squares) and high mass (filled circles) X-ray binaries. The origin of the coordinate is at the Galactic Centre. The Sun is located at $x=0$, $y=8.5$ (marked by the pentagon). The thin solid line shows logarithmic 4-armed ($m=4$) spiral model with pitch angle of 12° (e.g. Vallée (1995)). The thick solid lines show the spiral model of the Galaxy based on optical and radio observation of the giant HII regions (Georgelin & Georgelin (1976), Taylor & Cordes (1993)). The fact that the majority of sources is located at $y > 0$ is due to the flux limited nature of the ASM sample and incompleteness of the optical identifications/distance measurements at the large distances from the Sun (see discussion in the text).

take the model of Bahcall & Soneira (1980):

$$\rho_{Bulge} = \rho_{0,Bulge} \cdot \left(\frac{\sqrt{r^2 + \frac{z^2}{q^2}}}{r_0} \right)^{-\gamma} \cdot \exp\left(-\frac{r^2 + \frac{z^2}{q^2}}{r_t^2}\right) \quad (4)$$

$$\rho_{Disk} = \rho_{0,Disk} \cdot \exp\left(-\frac{r_m}{r} - \frac{r}{r_d} - \frac{|z|}{r_z}\right) \quad (5)$$

$$\rho_{Sphere} = \rho_{0,Sphere} \cdot \frac{\exp(-b \cdot (\frac{R}{R_e})^{1/4})}{(\frac{R}{R_e})^{7/8}}, \quad (6)$$

where $\rho_{0,Bulge}$, $\rho_{0,Disk}$ and $\rho_{0,Sphere}$ are the normalisations, r is the distance in the plane from the galactic centre, z is the distance perpendicular to the galactic plane, and R is the distance from the galactic centre in spherical coordinates. All distances are in kiloparsec. Meaning and values for other parameters are given in Table 4.

In the standard Galaxy model the mass ratios of the components are about 2:1:0.3 for disk:bulge:spheroid.

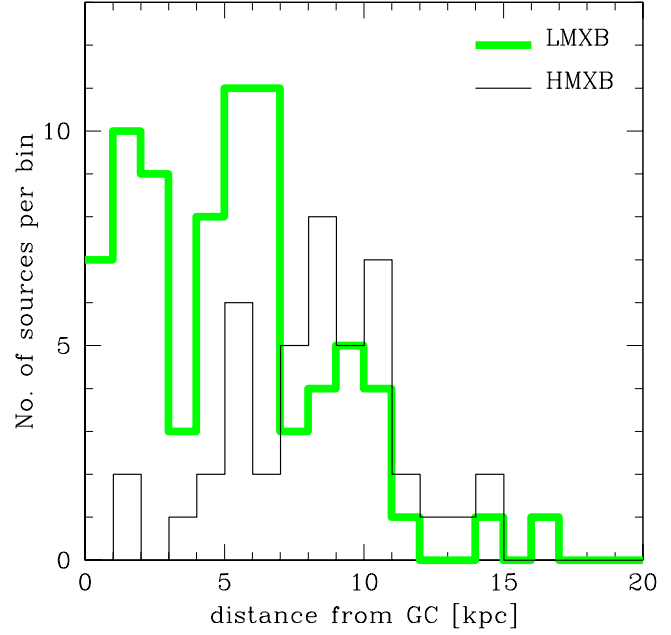


Fig. 8. Radial distributions of high mass (solid histogram) and low mass (thick grey histogram) X-ray binaries. The projected distance is defined as $\sqrt{x^2 + y^2}$, where x and y are Cartesian coordinates in the Galactic plane, see Fig. 7. Note that the plotted distributions are not corrected for the volume of cylindrical shells ($\propto r$).

These numbers follow from the model using normalisations for the disk, $\rho_{0,Disk} = 0.05 M_\odot \text{pc}^{-3}$, and spheroid population, $\rho_{0,Sphere} = 1/500 \cdot \rho_{0,Disk}$, observed in the vicinity of the Sun (Zombeck 1990) and a bulge mass of about $\sim 1.3 \cdot 10^{10} M_\odot$ (Dwek et al. 1995). All these masses refer to baryonic mass in the stars.

All three components of the standard Galaxy model were used to construct the spatial distribution of LMXB. The spheroid component with appropriately adjusted normalisation was used to account for the population of globular cluster sources. Based on the observed distribution and theoretical expectation that HMXBs trace the star forming regions in the Galaxy, only the disk component was used for the spatial distribution of HMXBs.

Several parameters, namely vertical scale height of the disk and relative normalisation of the spheroid for the LMXBs, can be determined directly from our sample of X-ray binaries. For these parameters we used the best fit values inferred by the data. For the rest of the parameters we accepted standard values for the stellar mass distribution in the Galaxy. The final set of the parameters is summarised in Table 4.

The disk component of the standard Galaxy model was modified in order to account for the Galactic spiral structure. The description of the spiral arms is based on the model of Georgelin & Georgelin (1976) derived from the distribution of HII regions. To include it into our Galaxy model we used the FORTRAN code provided by Taylor &

Cordes (1993). The spiral arms computed in this way are shown in Fig. 7 by thick grey lines. This empirical model is close but not identical to a 4 arm logarithmic spiral with pitch angle of 12° (e.g. Vallée (1995)) shown in Fig. 7 by thin solid lines.

In the following two subsections we discuss spatial distribution of HMXBs and LMXBs in more detail.

4.4. High mass X-ray binaries

The angular distribution of HMXBs in Fig. 6 shows signatures of the Galactic spiral structure. These signatures are clearly seen in the distribution of sources over galactic longitude which shows maxima approximately consistent with directions towards tangential points of the spiral arms. No significant peak in the direction to the Galactic centre is present. The signatures of the spiral structure become more evident in the 3-D distribution of the smaller sample of sources for which distance measurements are available, Figs. 7,8. The radial distribution (Fig. 8) shows pronounced peaks at the locations of the major spiral arms and is similar to that of primary tracers of the Galactic spiral structure – giant HII regions (e.g. Downes et al. (1980)) and warm molecular clouds (e.g. Solomon et al. (1985)). In particular, the central $\sim 3 - 4$ kpc region of the Galaxy is almost void of HMXB well in accordance with the radial distribution of the giant HII regions and warm CO clouds. This appears to correspond to the interior of the 4-kpc molecular ring.

The vertical distribution of HMXBs is significantly more concentrated towards the Galactic Plane and sufficiently well described by a simple exponential with a scale height of 150 pc as shown in the left panel of Fig. 9.

Based on theoretical expectations and on the data shown in Fig. 1,6,8,9 we included only the disk component in the volume density distribution HMXBs. It is clear however that a simple exponential disk is not a good description for the radial distribution of HMXB. Therefore, following Dehnen & Binney (1998) we assumed the disk density distribution in the form given by Eq. (5), where the first term in the exponential allows for the central density depression. To describe the observed central depression for HMXBs a rather large value of $r_m \approx 6 - 7$ kpc is required (cf. $r_m = 4$ kpc from Dehnen & Binney (1998)). The spiral arms were assumed to have a Gaussian density profile along the Galactic Plane:

$$\rho_{\text{Spiral}} \propto \sum_{j=1}^{j=4} \exp\left(-\left(\frac{s_j}{w_a}\right)^2\right), \quad (7)$$

where $w_a = 600$ pc is the width of the spiral arm, and s_j is the distance to the nearest point of the spiral arm j projected to the Galactic Plane:

$$s_j = \sqrt{(x - x'_j)^2 + (y - y'_j)^2}. \quad (8)$$

In order to account for the spiral structure the disk density, Eq. (5), was multiplied by ρ_{Spiral} :

$$\rho_{\text{Disk}}^{\text{HMXB}} \propto \rho_{\text{Disk}} \cdot \rho_{\text{Spiral}} \quad (9)$$

4.5. Low mass X-ray binaries

Contrary to HMXB, the angular distribution of LMXBs is strongly peaked in direction to the Galactic centre and declines gradually along the Galactic plane, see Fig. 6. The central ~ 2 kpc region is densely populated with Galactic Bulge LMXB sources and contains $\sim 1/3$ of the LMXBs from our flux limited sample (Fig. 8). A noticeable feature of the radial distribution of LMXB is the pronounced minimum at $\sim 3 - 4$ kpc. This minimum approximately coincides with the $\sim 1 - 3$ kpc gap in the distribution of the molecular gas and the ~ 2.2 kpc minimum in the density of infrared light distribution in the Galaxy (Binney et al. 1997) and probably separates bulge sources from the disk population. Similar to HMXBs, the signatures of the spiral structure might be present in the radial distribution although they are less pronounced.

The vertical distribution outside the bulge (Fig. 9) is significantly broader than that of HMXBs and includes a number of sources at high galactic z . A formal fit to the observed distribution with an exponential law results in a large scale height of 950 ± 130 pc, which is close to the value of 710 pc obtained by van Paradijs & White (1995) for NS LMXBs. However, due to presence of a tail of sources at $|z| > 1.5 - 2$ kpc, the observed z -distributions cannot be adequately described by a simple exponential law. As only three out of nine sources at $|z| > 2$ kpc are located in globular clusters, this tail of high- z sources cannot be solely due to the globular cluster component. A possible mechanism – a kick received by a compact object during the SN explosion, was considered e.g. by van Paradijs & White (1995). The relatively small number of high- z sources does not allow one to determine the shape of their distribution based on the data only. In order to account for the high- z sources and the LMXB sources in globular clusters we chose to include in the spatial distribution of LMXBs the spheroid component described by a de Vaucouleurs profile (Eq. (6)). Note that a de Vaucouleurs profile correctly represents the distribution of globular clusters. The overall vertical distribution can be adequately represented by a sum of an exponential law with a scale height of 410_{-80}^{+100} pc and a de Vaucouleurs profile with the parameters given in Table 4. The spheroid component represented by the de Vaucouleurs profile contains a $\sim 25\%$ of the total number of LMXBs. Note, that this number is by a factor of $\sim 2 - 3$ larger than the mass fraction of the stellar spheroid in the standard Galaxy model. The enhanced fraction of the spheroid component is generally consistent with the fact, that the number of X-ray sources per unit mass is ~ 100 times higher in the globular clusters than in the Galactic disk and 12 out of 104 LMXBs in our sample are globular cluster sources.

The angular resolution of the ASM instrument does not permit to study in detail the very central region of the Galaxy which is characterised by the highest volume and surface density of X-ray binaries. Based on GRANAT/ART-P data having significantly better sensitivity and angular resolution, Grebenev et al. (1996)

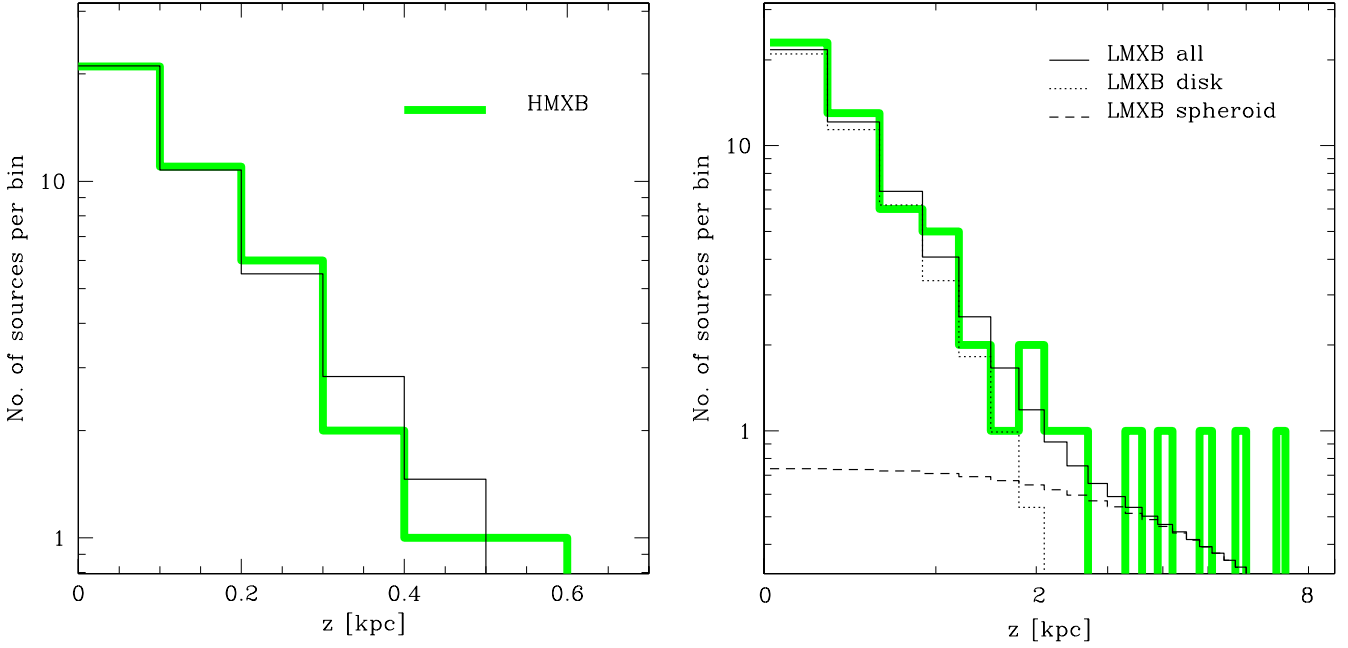


Fig. 9. Vertical distributions of high mass (left panel) and low mass (right panel) X-ray binaries. The vertical distributions were summed over northern and southern galactic hemispheres. In the case of LMXBs only sources with $R > 3.5$ kpc were used, to exclude bulge sources. The thick grey solid lines show the observed distributions and the thin solid and dashed lines the expected distributions for an exponential disk with 150 pc scale height for HMXBs, and an exponential with scale height 410 pc and a 25% contribution of the spheroid for LMXBs, respectively. For the assumed model see Eqs. (5, 6).

showed that the distribution of the surface density of X-ray binaries in the central $8^\circ \times 8^\circ$ of the Galaxy is consistent with the stellar mass distribution in the Galactic Bulge.

To conclude, our model of the volume density distribution of LMXBs includes all three components of the standard model of the Galaxy: bulge, disk and spheroid with the disk-to-spheroid mass ratio decreased to 4:1. Similarly to HMXBs, $r_m \approx 6 - 7$ kpc is required to describe the central density suppression of the disk population. The modulation of the disk component by the spiral pattern at the 20% level was also included:

$$\rho_{Disk}^{LMXB} \propto \rho_{Disk} \cdot (1 + 0.2 \cdot \rho_{Spiral}) \quad (10)$$

where ρ_{Disk} is given by Eq. (5) and ρ_{Spiral} – by Eq. (7).

4.6. Completeness of the sample of the distance measurements.

The fact that the majority of the sources in Fig. 7 is located at $y > 0$ is related to the flux limited nature of the ASM sample (obviously it is easier to observe weak sources located closer to the Sun) and to the incompleteness of the available distance measurements (more difficult to measure the distance to a more distant source). The 3-D distribution of X-ray binaries enables one to check the latter effect.

Plotted in Fig. 10 is the distribution of LMXB sources with luminosities $L_X > 4 \cdot 10^{36}$ erg s $^{-1}$ over the distance from the Sun. For the ASM completeness flux limit of 0.2 cts s $^{-1}$, sources with $L_X > 4 \cdot 10^{36}$ erg s $^{-1}$ should be visible up to a distance of ≈ 20 kpc. However, comparison with the expected distribution computed using the LMXB volume density distribution constructed in Sect. 4.5 shows an increasing deficiency of sources at distances $\gtrsim 10 - 15$ kpc. In total ~ 14 sources in the distance range of 10-20 kpc are “missing”. These “missing” sources should be hidden among the ~ 20 unclassified sources in the ASM catalogue for which no optical identification/distance determinations are available.

Recent observations by Kuijken & Rich (2001) lend support to this interpretation. They measured proper motions of blue and red giants in direction to the Galactic centre. The red giants, concentrated in the Galactic bulge, have a velocity dispersion in Galactic coordinates, b^{II} versus l^{II} , symmetric around zero. However, blue giants, located in the disk, have a velocity dispersion asymmetric around zero with respect to l^{II} which means that there is a net motion of the observed blue giants in one direction. Interpreting this as the motion of the disk around the Galactic centre, it also means that there is a deficit of the observed blue giants on the far side of the Galaxy (c.f. Fig. 10).

This comparison (Fig. 10) shows that our sample of optical identifications/distance measurements for LMXB

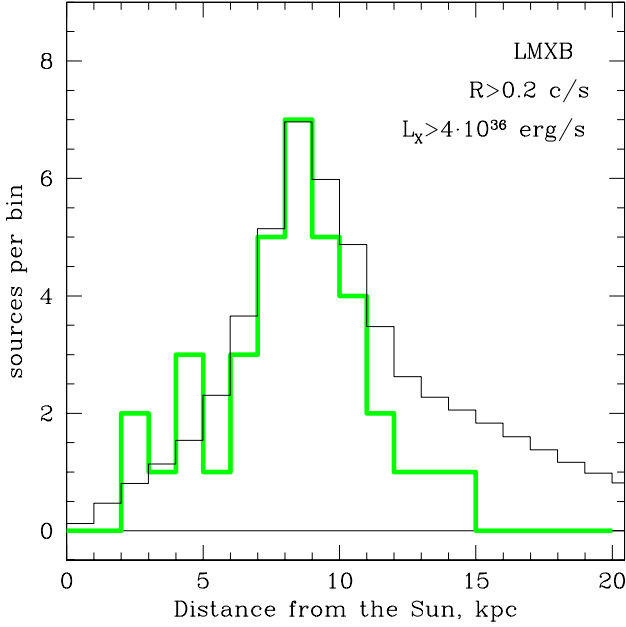


Fig. 10. Distribution of the LMXB sources over distance from the Sun (thick grey histogram). Only sources with luminosity $L_X > 4 \cdot 10^{36} \text{ erg s}^{-1}$ are plotted. Given the ASM completeness flux limit of 0.2 cnts s^{-1} , sources with $L_X > 4 \cdot 10^{36} \text{ erg s}^{-1}$ should be visible from the distance of upto $\approx 20 \text{ kpc}$. The thin solid histograms shows the expected distribution of the sources in the model constructed in Sect. 4.5. Deviation of the observed distribution from the prediction becomes visible at the distance $> 10 - 15 \text{ kpc}$.

sources is complete up to a distance of $\sim 10 \text{ kpc}$. The significantly smaller number of HMXBs above the ASM completeness flux limit did not permit us to perform a similar analysis for HMXB sources. However, one might expect that due to the higher luminosity of the optical companion the limiting distance for HMXBs is not smaller than for LMXBs. We therefore accepted a value of $D_{max} = 10 \text{ kpc}$ as a maximum source distance for the luminosity function calculation for both types of sources described in the next section.

5. Luminosity function

Due to the flux limited nature of the ASM sample and incompleteness of the optical identifications/distance measurements beyond $\sim 10 \text{ kpc}$, the *apparent* luminosity function which can be derived straightforwardly from the ASM flux measurements and the source distances (thin line histograms in Fig. 12 and 13) needs to be corrected for the fraction of the Galaxy observable by ASM. This correction can be performed using the model of the spatial distribution of X-ray binaries constructed in the previous section:

$$\frac{dN}{dL} = \left(\frac{dN}{dL} \right)_{\text{obs}} \times \frac{M(< D(L))}{M_{\text{tot}}} \quad (11)$$

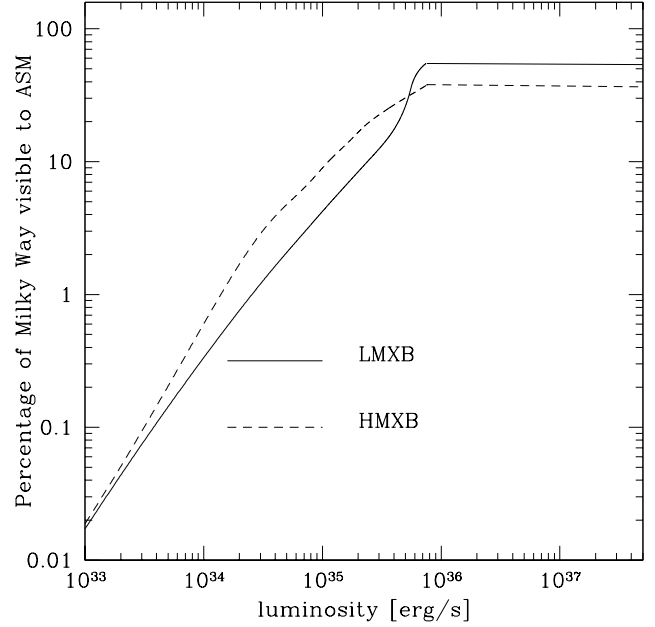


Fig. 11. Fraction of the mass of the Galaxy visible to ASM with account for the selection criteria described in the text as a function of source luminosity.

where $\frac{dN}{dL}$ is the true luminosity function, $\left(\frac{dN}{dL} \right)_{\text{obs}}$ – apparent luminosity function constructed using ASM flux measurements and the source distances, $M(< D)$ – mass of the Galaxy inside distance D from the Sun computed using the volume density distributions for HMXB and LMXB sources from the Sect. 4, M_{tot} – total mass of the Galaxy, $D(L)$ is defined by:

$$D(L) = \min \left(\frac{L}{\sqrt{4\pi F_{lim}}}, D_{max} \right) \quad (12)$$

where F_{lim} is the limiting (minimum) flux and D_{max} – the maximum distance from the Sun of the sources used for constructing the luminosity function. As discussed in the previous sections we accepted the following selection criteria: $F_{lim} = 0.2 \text{ cnts s}^{-1} \approx 6.4 \cdot 10^{-11} \text{ erg s}^{-1} \text{ cm}^{-2}$, i.e. equal to the completeness flux limit of the ASM catalogue, and $D_{max} = 10 \text{ kpc}$ – a completeness limit of distance measurements estimated in Sect. 4.6.

Obviously, for a given flux limit F_{lim} the mass fraction of the Galaxy $\frac{M(< D(L))}{M_{\text{tot}}}$ is a decreasing function of the source luminosity as shown in Fig. 11. For the ASM sensitivity/completeness limit of $\approx 6.4 \cdot 10^{-11} \text{ erg s}^{-1} \text{ cm}^{-2}$ the entire volume inside $D_{max} = 10 \text{ kpc}$ from the Sun is observable down to a luminosity of $\approx 10^{36} \text{ erg s}^{-1}$ (the flat part of the curves in Fig. 11) below which the mass fraction of the observable part of the Galaxy begins to decrease. As the spatial distributions of HMXB and LMXB sources differ significantly, the volume correction and the luminosity function were calculated separately for HMXBs and LMXBs. The apparent and volume corrected (true) cumulative luminosity functions are presented in Fig. 12.

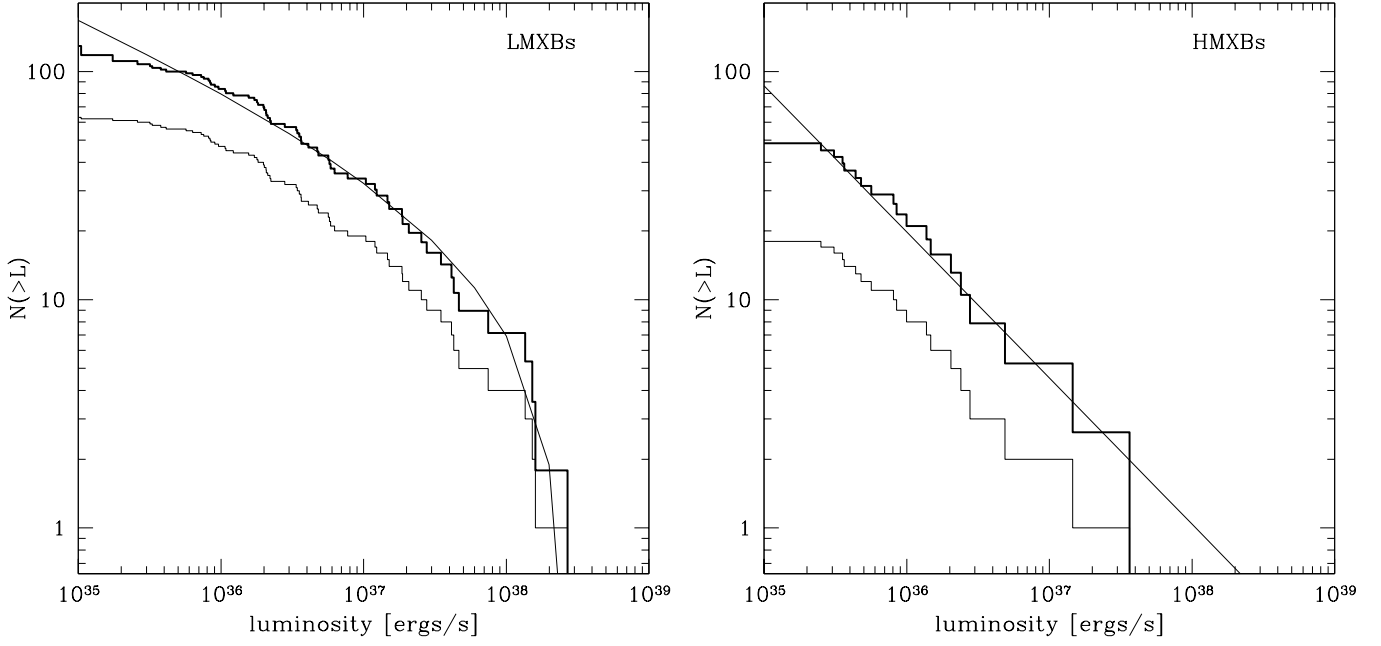


Fig. 12. The apparent (thin histogram) and volume corrected (thick histogram) cumulative luminosity function for LMXBs and HMXBs. The solid lines are the best fits to the data.

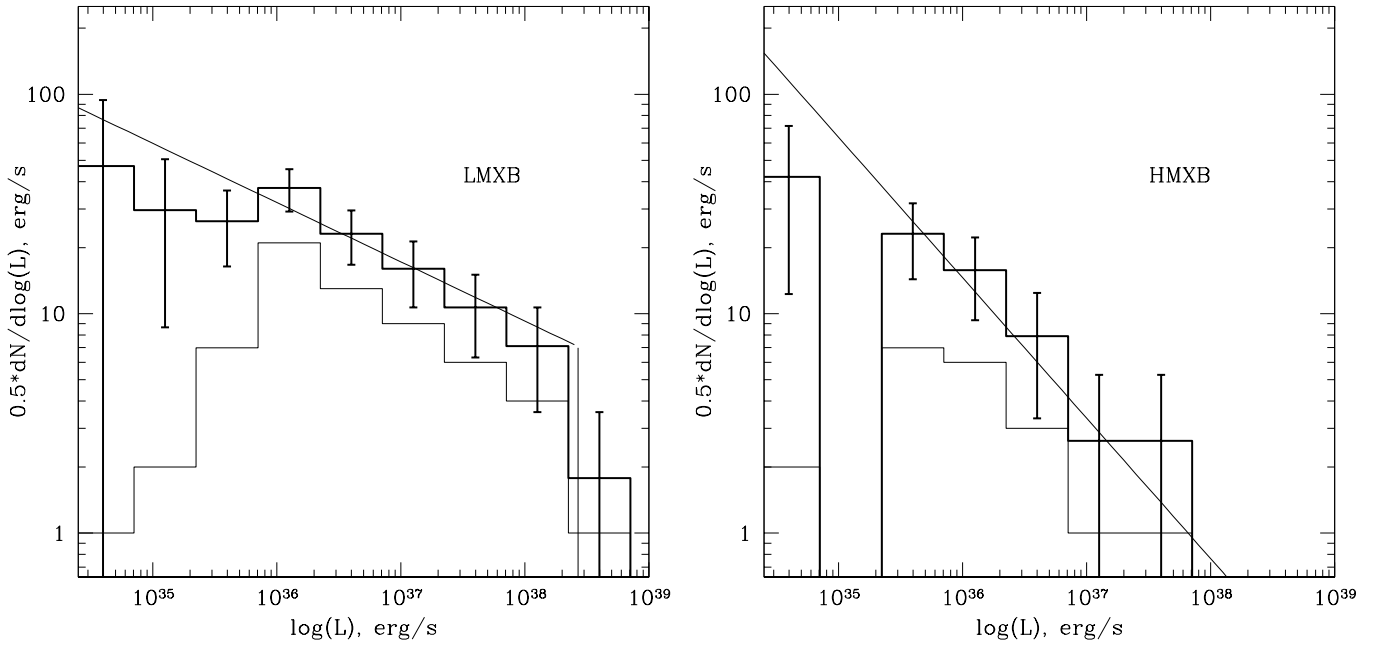


Fig. 13. The apparent (thin histogram) and volume corrected (thick histogram) differential luminosity function for LMXBs and HMXBs binned into bins with logarithmic width of 0.5. The solid lines are the best fits to the cumulative distributions. The fall-over of the apparent distributions below $\sim 10^{36}$ erg s $^{-1}$ are due to the flux limited nature of the ASM sample (see Fig. 11)

Fig. 13 shows the corresponding differential distributions binned logarithmically over luminosity.

The cumulative luminosity function of HMXBs (Fig. 12, right panel) does not seem to contradict to a power law distribution down to a luminosity of $\sim 2 \cdot 10^{35}$ erg s $^{-1}$ with

some indication of flattening at lower luminosity. However, limited sensitivity of ASM and correspondingly large values of the correction factor (Fig. 11) at low luminosities do not allow one to draw a definite conclusion regarding the shape of the luminosity function at these low lumi-

nosities (see comparison with ASCA source counts in Sec. 7). We therefore fitted the luminosity function of HMXBs in the $L > 2 \cdot 10^{35} \text{ erg s}^{-1}$ range with a power law distribution. Using a Maximum-Likelihood method the best fit parameters are:

$$N(> L) = 20 \cdot \left(\frac{L}{10^{36} \text{ erg s}^{-1}} \right)^{-0.64 \pm 0.15} \quad (13)$$

where L is the source luminosity in erg s^{-1} and $N(> L)$ – total number of sources on the sky with luminosity greater than L .

The shape of both cumulative and differential luminosity function for LMXBs (Figs. 12, 13, left panels) indicates the presence of a high luminosity cut-off. We fitted the unbinned cumulative distribution with the functional form

$$N(> L) = A \cdot (L^{-\alpha} - L_{max}^{-\alpha}). \quad (14)$$

corresponding to a power law differential luminosity function with a sharp cut-off at L_{max} . The value of the cutoff was set equal to $2.7 \cdot 10^{38} \text{ erg s}^{-1}$ which corresponds to the luminosity of the most luminous source within 10 kpc, Sco X-1. The best fit values of other parameters are:

$$N(> L) = 105 \cdot \left(\left(\frac{L}{10^{36} \text{ erg s}^{-1}} \right)^{-0.26 \pm 0.08} - 270^{-0.26} \right). \quad (15)$$

Note that the smaller number of sources and the steeper slope of luminosity function make the HMXB data insensitive to a high luminosity cut-off above $\sim \text{few} \times 10^{36} \text{ erg s}^{-1}$.

5.1. Effect of the Galaxy model on the luminosity function

From Eq. (11) it is clear that the luminosity function depends on the spatial distribution of XRBs in the Galaxy. As discussed above, using the distance measurements available, we were able to determine some of the parameters of their distribution. But the data are not sufficient to determine the entire distribution unambiguously. Thus we had to assume a spatial distribution of XRBs in the Galaxy. In order to investigate the effect of the adopted spatial distribution of X-ray sources on the derived luminosity function we varied our model and computed the respective luminosity functions.

For our analysis we used three different distributions for LMXBs and HMXBs. In the case of HMXBs, only the disk component was included in each of the three distributions. The modulation of the disk distribution by the spiral pattern, when present, was 100% for HMXB and 20% for LMXB. The models are:

- Model A: Our primary model constructed in Sec. 4 and used to derive the luminosity function above (shown as a solid histogram in Fig. 14).

- Model B: The same as the model A, except that the inner cut-off of the disk was set to $r_m = 4 \text{ kpc}$ in accordance with the result of Dehnen & Binney (1998) (dotted histogram in Fig. 14).
- Model C: The spheroid component is the same as in Model A. The disk radial distribution is without the inner cut-off, i.e. $r_m = 0$ and without modulation by the spiral structure. No bulge component is included for either LMXBs or HMXBs. The resulting density distribution is similar to that derived by van Paradijs & White (1995) for NS LMXBs (dashed histogram in Fig. 14).

The resulting luminosity function for each of the three models are shown in Fig. 14. It is obvious that there is no strong dependence of the luminosity function on the mass distribution. The slopes vary in the range from 1.28 – 1.30 for LMXBs and 1.64 – 1.72 for HMXBs. The total number of sources varies from 88 to 90 for LMXBs and from 21 to 26 for HMXBs. It is worth noting that the spiral pattern is no significant factor in the determination of the luminosity function of HMXBs although the spatial distribution shows clear signs of them.

5.2. Total X-ray luminosity of Galactic X-ray binaries

The total luminosity of all X-ray binaries in the Galaxy is calculated in the following way. Down to a luminosity of $10^{36} \text{ erg s}^{-1}$ we sum the measured luminosities of the individual sources to obtain a more precise number. For the lower luminosities that contribute only a small fraction to the total luminosity we use the analytical description of the luminosity function given by Eqs. (13) and (15).

The integrated luminosity of HMXBs and LMXBs in the 2–10 keV ASM band calculated in such way are $\approx 2 \cdot 10^{38} \text{ erg s}^{-1}$ and $\approx 2.5 \cdot 10^{39} \text{ ergs s}^{-1}$, respectively. Note that these numbers refer to the luminosity *averaged* over the period from 1996–2000. The variability of individual sources or an outburst of a bright transient can change the luminosity by a factor of up to $\sim 2 - 3$. Due to the shallow slopes of the luminosity functions the integrated X-ray emission of the Milky Way is dominated by the $\sim 5 - 10$ most luminous sources (see Table 5 and 6). The maximum and minimum values for the luminosities were estimated by eye from the 1 day averaged light curves. The values in the tables therefore differ from the values in Table 1.

Normalised to the star formation rate which is about $4 \text{ M}_{\odot} \text{ yr}^{-1}$ in the Milky Way (McKee & Williams 1997) galactic HMXBs emit about $\sim 5 \cdot 10^{37} \text{ erg s}^{-1} / (\text{M}_{\odot} \text{ yr}^{-1})$. The luminosity of LMXBs normalised to the stellar mass is about $\sim 5 \cdot 10^{28} \text{ erg s}^{-1} \text{ M}_{\odot}^{-1}$, assuming a stellar mass of the Galaxy of about $5 \cdot 10^{10} \text{ M}_{\odot}$.

The contribution of Be X-ray binaries from the ASM sample to the integrated luminosity of HMXBs is $\sim 5\%$.

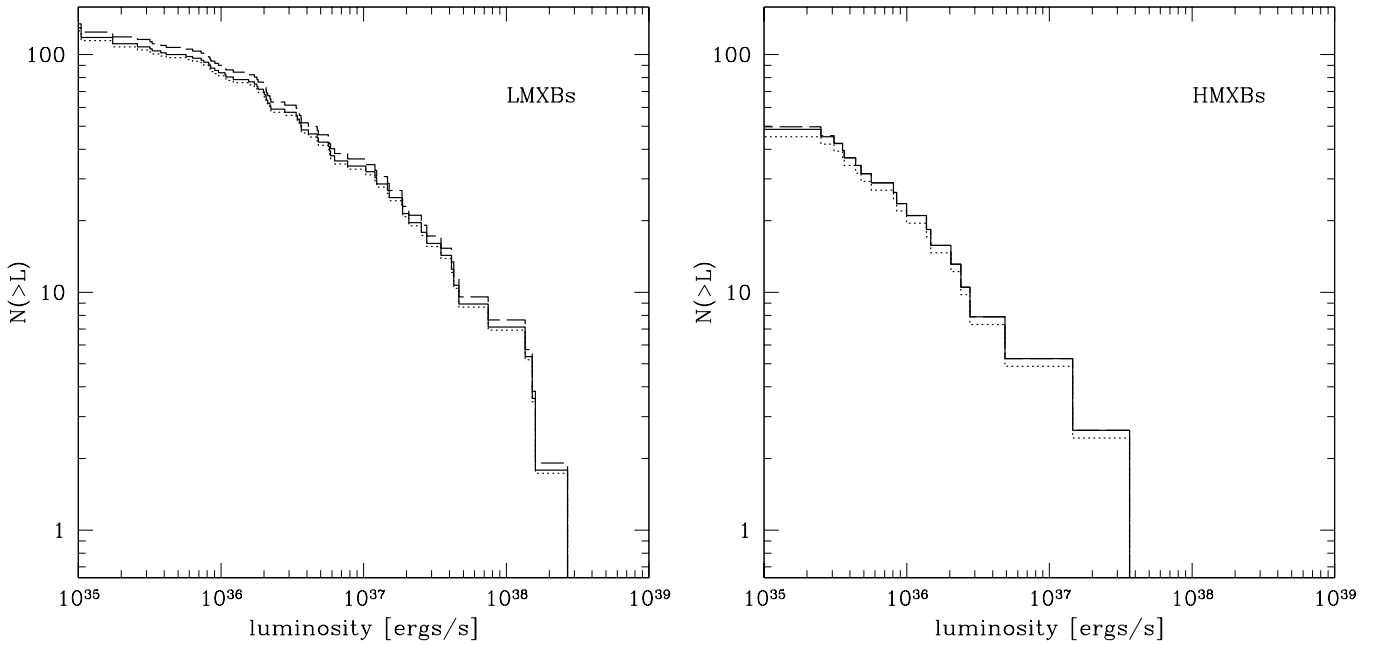


Fig. 14. Dependence of the luminosity function on the adopted model of the spatial distribution of XRBs. The figures show the luminosity functions of LMXBs (left panel) and HMXBs (right panel) for three different Galaxy models. The solid, dotted and dashed lines in both panels correspond to the models A, B and C.

Note that poor knowledge of the shape of the luminosity function at low luminosities, $L \lesssim 10^{35} \text{ erg s}^{-1}$ should not influence the total luminosity considerably unless the luminosity function steepens significantly at these low luminosities (see Sec. 7).

The total number of X-ray binaries above $2 \cdot 10^{35} \text{ erg s}^{-1}$ obtained from the luminosity functions is about ~ 190 of which ~ 55 are HMXBs and ~ 135 – LMXBs.

5.3. Luminosity function and \dot{M} distribution of X-ray binaries

The X-ray luminosity function is obviously related to the distribution of X-ray binary systems over the mass loss rate of the secondary, \dot{M} . The simplest assumption would be that both distributions have the same slope in the range corresponding to luminosities of $\sim (0.01 - 1)L_{Edd}$. At larger luminosities, $L \gtrsim L_{Edd}$, the luminosity function has a break or cut-off, well in accordance with theoretical expectation, that the luminosity due to accretion cannot exceed the Eddington luminosity of the primary star by a large factor (see discussion in Sect. 8). The donor star in a binary system, on the other hand, “does not know” about the Eddington critical luminosity, therefore the distribution of binary systems over the mass loss rate of the secondary, \dot{M} , is not expected to break near the Eddington value for the compact object. Thus the distribution of binary systems over \dot{M} is expected to continue with the same slope well beyond the Eddington value.

Extremely super-Eddington values of the mass accretion rate \dot{M} can result in quenching of the X-ray source

and/or its obscuration by the matter expelled from the system by radiation pressure (Shakura & Sunyaev 1973). This would lead to the appearance of a peculiar object, dim in X-rays and extremely bright in the optical and UV band – similar to SS 433 or the recent fast transient V4641 Sgr at the peak of its optical outburst. Such objects would emit only a negligible fraction in the X-ray band and would contribute to the lower luminosity end of the XRB luminosity function.

For moderately super-Eddington values of $\dot{M} \lesssim 10 - 100\dot{M}_{Edd}$, however, one might expect the appearance of a near- or slightly super-Eddington source, therefore all such systems are expected to cluster near L_{Edd} . For a given slope of the luminosity function the number of such sources can be easily estimated. For the observed parameters of the LMXB luminosity function (slope = 1.3, 42 sources with $36.5 < \log(L_X) < 38$) and assuming that the \dot{M} distribution continues with the same slope = 1.3, the total number of sources with \dot{M} corresponding to the range of luminosities of $10^{38} - 10^{39}$ and $10^{39} - 10^{40} \text{ erg s}^{-1}$ is ≈ 10 and ≈ 6 correspondingly (≈ 7 sources are expected to have \dot{M} corresponding to $L > 10^{40} \text{ erg s}^{-1}$). These estimates are in disagreement with the actually observed number of sources with $L \gtrsim 10^{38} \text{ erg s}^{-1}$, which is equal to 8. In order to reconcile the expected number of sources near L_{Edd} with the observations, a slope of the \dot{M} distribution of $\gtrsim 1.35 - 1.40$ is required which is somewhat steeper than the observed value of ~ 1.3 . We note that the slope of ~ 1.35 is within $\sim 1\sigma$ of the the observed value.

Finally, there are several effects that can suppress the number of the low luminosity sources, i.e. make the lumi-

Table 5. List of the most luminous LMXB sources contributing $\approx 90\%$ to the integrated luminosity of LMXBs in the 2–10 keV band, averaged over 1996–2000. The 12 most luminous sources contribute $\approx 80\%$ of the integrated luminosity.

Source	L_X [$10^{38} \text{ erg s}^{-1}$]			dist. [kpc]	Ref.
	avg.	min. ^(a)	max. ^(a)		
Cir X-1	4.4	0.3	10	10.9	1
GRS 1915+105	3.7	1	11	12.5	2
Sco X-1	2.7	2	4.5	2.8	3
Cyg X-2	1.8	0.9	3.4	11.3	1,4–7
GX 349+2	1.6	1.1	2.7	9.2	1,7,8
GX 17+2	1.5	1.1	2.4	9.5	1,7,9,10
GX 5-1	1.4	1	1.8	7.2	1,7
GX 340+0	1.3	0.9	1.8	11.0	1,7
GX 9+1	0.75	0.5	1.0	7.2	9
NGC 6624	0.47	0.15	0.8	8.0	10,11
Ser X-1	0.43	0.26	0.6	8.4	12
GX 13+1	0.41	0.25	0.6	7.0	13
X 1735-444	0.35	0.2	0.6	9.2	1
XTE J1550-564	0.35	0.005	2.1	5.3	14
KS 1731-260	0.28	0.06	0.6	8.5	15–17
X 1705-440	0.25	<0.04	0.6	7.4	18
X 1624-490	0.24	<0.13	0.4	13.5	9

^(a) min. and max. luminosity were estimated by eye from the 1 day averaged light curves.

References for the distances: (1) – van Paradijs & White (1995), (2) – Mirabel & Rodríguez (1994), (3) – Bradshaw et al. (1999), (4) – Orosz & Kuulkers (1999), (5) – Cowley et al. (1979), (6) – Smale (1998), (7) – Penninx (1989), (8) – Wachter & Margon (1996), (9) – Christian & Swank (1997), (10) – Djorgovski (1993), (11) – Webbink (1985), (12) – Ebisuzaki et al. (1984), (13) – Bandyopadhyay et al. (1999), (14) – ?, (15) – Barret et al. (1998), (16) – Smith et al. (1997), (17) – Sunyaev (1990), (18) – Haberl & Titarchuk (1995)

nosity function flatter than the \dot{M} distribution. The most obvious and important are discussed below.

- In the case of HMXBs the magnetosphere of the strongly magnetised, rapidly rotating neutron star can prevent the accretion at low \dot{M} via the propeller effect (Illarionov & Sunyaev 1975).
- Be-systems are characterised by regular outbursts corresponding to the passage of the neutron star through the equatorial stellar wind. Therefore for such sources the true value of the \dot{M} in the binary system is measured by the peak luminosity during the outbursts whereas the long term averaged luminosity, used to construct the luminosity function, can give a significantly underestimated value.
- A common property of LMXBs, containing both neutron stars and black hole, is the presence of relativistic jets which might carry away a sizable fraction of the energy of accretion (Mirabel & Rodríguez 1999). The presence of jets correlates with the X-ray spectral state: the jets are absent (and hence the true accretion efficiency is higher) in the soft spectral state corre-

Table 6. List of the most luminous HMXB sources that contribute $\approx 40\%$ to the integrated luminosity of HMXBs in the 2–10 keV band, averaged over 1996–2000.

Source	L_X [$10^{38} \text{ erg s}^{-1}$]			dist. [kpc]	Ref.
	avg.	min. ^(a)	max. ^(a)		
Cyg X-3	0.5	0.08	1.4	9.0	1
Cen X-3	0.15	<0.03	0.7	9.0	2–5
Cyg X-1	0.05	0.02	0.17	2.1	6
X 1657-415	0.043	<0.02	0.22	11.0	7
V4641 Sgr	0.028	<0.02	7.3	9.9	8
GX 301-2	0.02	< 0.005	0.4	5.3	9
XTE J1855-024	0.015	<0.01	0.11	10.0	10
X1538-522	0.014	< 0.008	0.08	6.4	11
GS1843+009	0.01	< 0.007	0.11	10.0	12
X1908+075	0.008	< 0.006	0.05	6.4	13, 14

^(a) min. and max. luminosity were estimated by eye from the 1 day averaged light curves.

References for the distances: (1) – Predehl et al. (2000), (2) – Krzeminski (1974), (3) – Hutchings et al. (1979), (4) – Motch et al. (1997), (5) – Bahcall (1978), (6) – Massey et al. (1995), (7) – Chakrabarty et al. (1993), (8) – Orosz et al. (2000), (9) – Kaper et al. (1995), (10) – Corbet et al. (1999), (11) – Reynolds et al. (1992), (12) – Israel et al. (2001), (13) – Wen et al. (2000), (14) – van Paradijs & White (1995)

sponding to higher values of \dot{M} . The jets exist only in the hard spectral state (Fender 2001), thus decreasing the accretion efficiency at lower \dot{M} .

- In the case of black hole binaries an ADAF can form at low accretion rate in which case the accretion efficiency is proportional to \dot{M} and the X-ray luminosity scales as $L \propto \dot{M}^2$ (Narayan & Yi 1995).
- At sufficiently low accretion rates a source becomes a transient with a recurrence time varying from ~ 1 to $\gtrsim 50$ years (White et al. 1984). This would decrease the number of low and intermediate luminosity sources in the luminosity function constructed on the several years baseline.

The number of luminous X-ray binaries in the Milky Way is insufficient to study the shape of the luminosity function near L_{Edd} in detail. On the other hand within next several years CHANDRA X-ray observatory will study compact sources in a large number of nearby, $d \lesssim 50$ Mpc galaxies and the total number of the X-ray binaries detected in other galaxies can easily reach several hundred or thousand. In this context it might be interesting to construct a combined luminosity function of X-ray binaries in our and other galaxies to study its exact shape at the high luminosity end and search for a possible excess of sources near L_{Edd} .

6. Comparison with nearby galaxies

The total luminosity of X-ray binaries in the Milky Way, $\sim 2-3 \cdot 10^{39} \text{ erg s}^{-1}$ in the 2–10 keV band, agrees sufficiently well with observations of M 31, for which GINGA has

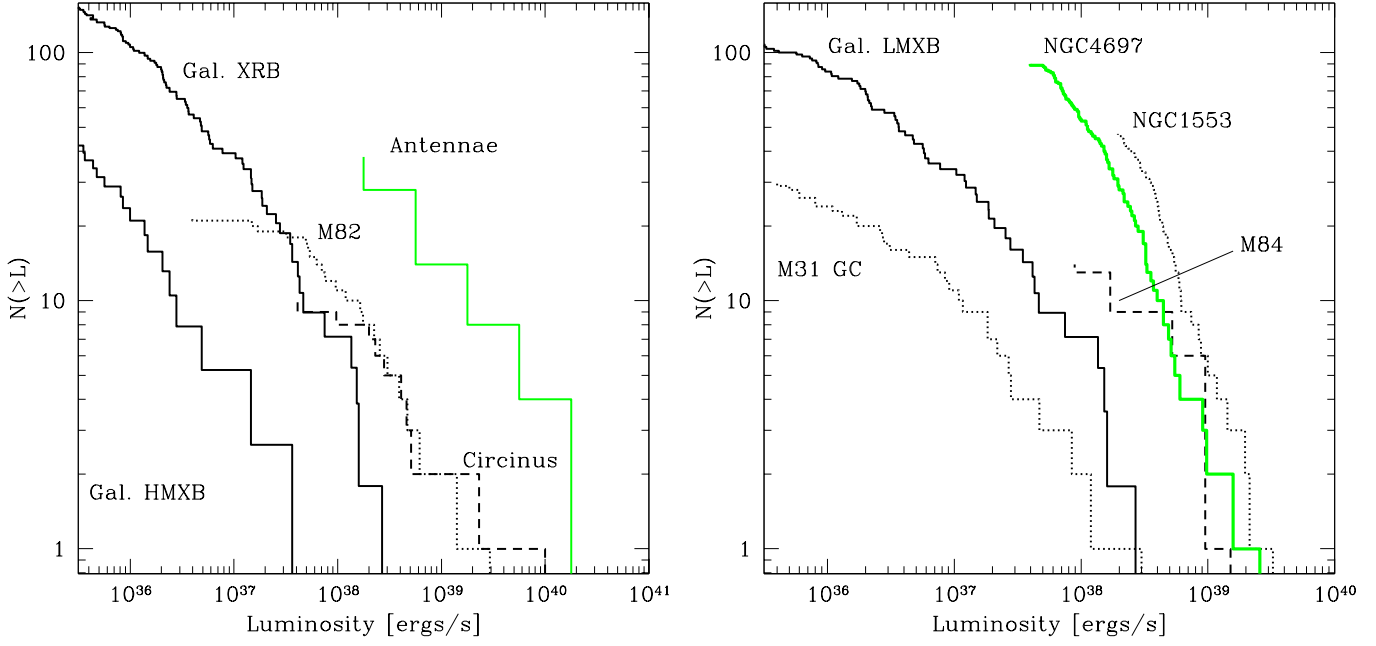


Fig. 16. Cumulative luminosity functions of galaxies observed with CHANDRA. The left panel shows actively star forming spiral galaxies that include NGC 4038/39 and M 82 which are supposed to be dominated by HMXBs. For comparison the luminosity functions of Galactic X-ray binaries and HMXBs alone are shown. The right panel shows elliptical galaxies including the SO galaxy NGC 1553. For comparison the luminosity function of Galactic LMXBs is shown.

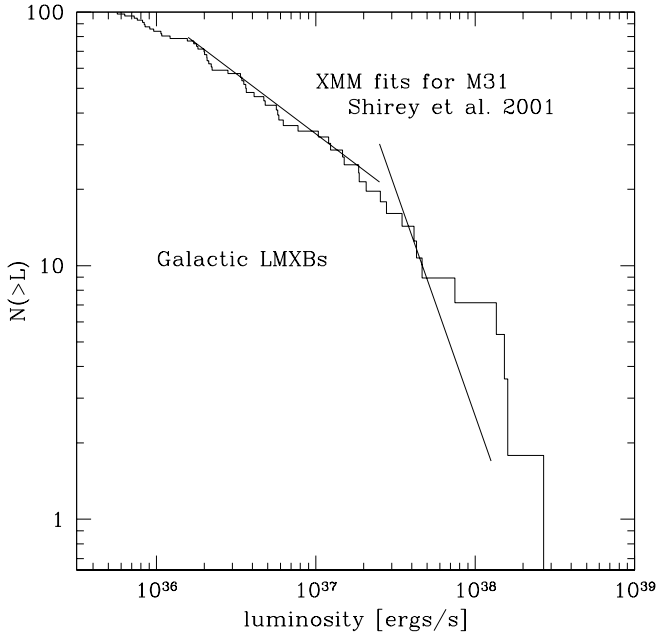


Fig. 15. Cumulative luminosity function of Galactic LMXBs and also the best fit values for the XMM-Newton observation of M 31 by Shirey et al. (2001)

found a luminosity of $5 \cdot 10^{39}$ ergs s $^{-1}$ between 2-20 keV (Makishima et al. 1989).

Recently XMM-Newton observed the inner 30' region of M 31 (Shirey et al. 2001). In total 116 sources were detected above the limiting luminosity of $6 \cdot 10^{35}$ erg s $^{-1}$ in the 0.3–12 keV energy range, assuming a distance of 760 kpc. Shirey et al. (2001) distinguish between two luminosity ranges, $36.2 < \log(L_X) < 37.4$, for which the best fit slope is -0.47 ± 0.03 , and $37.4 < \log(L_X) < 38.1$ where the best fit slope is -1.79 ± 0.26 . At the distance of 760 kpc 30' correspond to ≈ 6.6 kpc therefore these data should be compared with the luminosity function of Galactic LMXBs, assuming that similarly to the Milky Way the inner part of M31 is populated mainly with LMXBs. The two luminosity functions are plotted in Fig. 15. Although the general shapes of the luminosity functions of LMXBs in the Milky Way and in M 31 are similar, it is obvious that one can not be obtained from the other by a shift along the vertical axis as one would expect if the luminosity function was simply proportional to the mass of the host galaxy.

CHANDRA observations have produced luminosity functions of compact sources in a number of nearby galaxies, including ellipticals: NGC 4697 (Sarazin et al. 2000), M 84 (Finoguenov & Jones 2001) and NGC 1553 (Blanton et al. 2001), spirals: M 81 (Tennant et al. 2001), Circinus (Smith & Wilson 2001), M31 (Garcia et al. 2000) and starburst galaxies: NGC 4038/39 (Antennae) (Fabbiano et al. 2001) and M 82 (Griffiths et al. 2000). The luminosity functions of the compact sources in these galaxies are compared to that of the Milky Way in Fig. 16. The

left panel in Fig. 16 shows spirals and starbursts which are expected to have a higher fraction of HMXBs due to higher star formation rates. These are compared with the luminosity functions of HMXBs and all X-ray binaries in the Milky Way. The right panel in Fig. 16 shows elliptical galaxies along with the luminosity function of Galactic LMXBs.

As the example of our Milky Way shows, X-ray binaries in globular clusters play an important role in determination and understanding the properties of the population. It is also well known that globular cluster systems are quite different for early- and late-type galaxies, in terms of number per galaxy luminosity (Harris & Racine 1979) as well as depend on the environment of the host galaxy (Bridges & Hanes 1990). Taken together this shows the need for a closer study of X-ray binaries in globular clusters – ideally they should be treated separately, when studying the luminosity function of LMXB sources. Unfortunately only for few galaxies there are observations which allow the separation of globular cluster X-ray sources, e.g. M 31 (Di Stefano et al. 2002) and NGC 1399 (Angelini et al. 2001). We therefore decided to ignore in the present study the possible effects of the globular cluster sources on the overall luminosity function.

Comparing the HMXB luminosity function in our and nearby star forming galaxies we could check the proportionality of the HMXB luminosity to star forming rate. There might be several additional factors involved including chemical abundance of the particular galaxy. For example, the HMXB sources in LMC and SMC appear to be significantly more luminous than the HMXB sources in our Galaxy, even though the star formation rates are comparable. Especially interesting is the case of the Antennae galaxies where the difference from the Galactic HMXB luminosity function is extremely impressive. It seems that it can not be explained simply by the difference in the star formation rate, which is about 20 times higher (Neff & Ulvestad 2000) whereas the number of X-ray sources is a factor of more than 50 higher. This example shows that the knowledge of the HMXB luminosity function seems to be insufficient to measure the star formation rate in galaxies and to estimate the distances to them with acceptable precision.

CHANDRA observations are also opening an important possibility to check the proportionality of LMXB luminosity functions to the mass of the parent galaxies.

7. Low luminosity sources

7.1. Extension of $\text{Log}(N)$ – $\text{Log}(S)$ towards lower fluxes

Since the sensitivity of ASM is limited to relatively high flux sources it is interesting to investigate the behaviour of the $\text{Log}(N)$ – $\text{Log}(S)$ at lower fluxes. Note that, given the slope observed by ASM (1.2 and 1.61 for LMXBs and HMXBs), the $\text{Log}(N)$ – $\text{Log}(S)$ distribution should flatten at low fluxes since the total number of sources in the Galaxy is finite.

In order to study the low flux regime below the ASM completeness limit of $\approx 6.4 \cdot 10^{-11} \text{ erg s}^{-1} \text{ cm}^{-2}$, we use ASCA data from the Galactic Ridge Survey (Sugizaki et al. 2001) covering ≈ 40 square degrees with the limiting sensitivity of $\sim 3 \cdot 10^{-13} \text{ erg s}^{-1} \text{ cm}^{-2}$. Since most of the sources in the ASCA survey are unidentified we followed the criterion suggested by Sugizaki et al. (2001) in order to discriminate X-ray binary candidates from other sources: that X-ray binary candidates have either a spectral photon index $\Gamma < 1$, or a spectral photon index $\Gamma < 3$ and a column density $N_H < 0.8 \cdot 10^{22} \text{ cm}^{-2}$. Excluding otherwise identified sources with these spectral properties there remain 28 sources. We fit the $\text{Log}(N)$ – $\text{Log}(S)$ of the selected sources with the procedure similar to that used for ASM sources, modified to account for the flux dependent sky coverage of the ASCA survey (Fig. 7 in Sugizaki et al. (2001)). The resulting $\text{Log}(N)$ – $\text{Log}(S)$ is:

$$N(> S) = 9.4 \cdot 10^{-5} \cdot S^{-0.42 \pm 0.08} \quad (16)$$

where S is flux in units of $10^{-12} \text{ erg s}^{-1} \text{ cm}^{-2}$. To compare ASCA data with an extrapolation of the ASM number–flux relation one needs to account for the difference in their sky coverage ($|l| \lesssim 40^\circ$ and $|b| \lesssim 0.3^\circ$ for ASCA survey and entire sky for the ASM data). An approximate value of the correction factor can be estimated as the fraction of the mass of the Milky Way covered by the ASCA Galactic Ridge Survey with account for its sensitivity and the particular pattern of its sky coverage (Fig. 1 in Sugizaki et al. (2001)). The mass fraction was calculated using the Galaxy model described in Sect. 4 and equals to $\sim 1:21$. Converting the cumulative $\text{Log}(N)$ – $\text{Log}(S)$ to differential $\text{Log}(N)$ – $\text{Log}(S)$ for ASCA X-ray binary candidates and all ASM X-ray binaries and multiplying the resulting ASCA $\text{Log}(N)$ – $\text{Log}(S)$ by 21 we obtain the result shown in Fig. 17.

It is obvious that the agreement between ASM and ASCA data is sufficiently good. The slopes are different at the $\sim 2\sigma$ level. On the other hand since the sources are all unidentified and their distances unknown it is not possible to distinguish between high and low mass X-ray binaries which have different slopes of their $\text{Log}(N)$ – $\text{Log}(S)$ distributions in the ASM sample. Indeed, due to the small range in Galactic latitude b^{II} covered by the ASCA survey and due to the fact that HMXBs have a 3 times smaller vertical scale height (cf. Sec. 4), the ratio of HMXBs to LMXBs should be different for the ASCA and ASM samples. The fraction of HMXBs, having steeper $\text{Log}(N)$ – $\text{Log}(S)$, should be larger in the ASCA sample and thus the resulting $\text{Log}(N)$ – $\text{Log}(S)$ should be somewhat steeper. We conclude that the data of the ASCA Galactic Ridge Survey indicate that there are no significant deviations in the $\text{Log}(N)$ – $\text{Log}(S)$ from the extrapolations of the ASM data down to the sensitivity limit of the ASCA survey of $\sim 5 \cdot 10^{-13} \text{ erg s}^{-1} \text{ cm}^{-2}$.

7.2. Low luminosity end of X-ray binary luminosity function

Knowledge of the $\text{Log}(N)\text{--}\text{Log}(S)$ observed by ASCA and the spatial distribution of sources in the Galaxy gives a possibility to constrain the low luminosity end of the luminosity function. If the luminosity function observed with ASM continues to lower luminosities then it should be possible to reproduce the $\text{Log}(N)\text{--}\text{Log}(S)$ observed by ASCA according to the formula

$$N(> S) = \int_{L_{\min}}^{L_{\max}} \frac{dN}{dL} \cdot \frac{M(< r)_{\text{ASCA}}}{M_{\text{total}}} dL, \quad (17)$$

with

$$r = \sqrt{\frac{L}{4\pi \cdot S}}. \quad (18)$$

where $N(> S)$ is the number of sources with a flux higher than S observed by ASCA, $\frac{dN}{dL}$ is the differential luminosity function, and $\frac{M(< r)_{\text{ASCA}}}{M_{\text{total}}}$ is the fraction of mass within a radius r from the Earth within the field of view of the ASCA survey, L_{\max} is the high luminosity cut-off of the luminosity function (Eqs. (13) and (15)). The L_{\min} is the low luminosity cut-off of the luminosity function below which it is assumed to be equal to zero. This quantity characterises roughly the luminosity level at which the luminosity function deviates significantly from the extrapolation of the ASM power law.

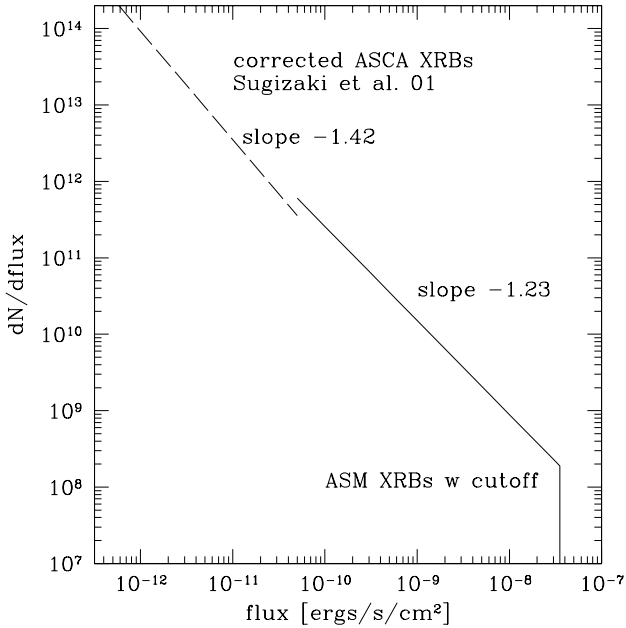


Fig. 17. Comparison of the differential $\text{Log}(N)\text{--}\text{Log}(S)$ relation for Galactic X-ray binaries obtained by ASM (solid line with break) and by ASCA Galactic Ridge Survey (dashed line). The ASCA number–flux relation was multiplied by an approximate correction factor accounting for the difference in the sky coverage of the ASM and ASCA surveys (see text for details).

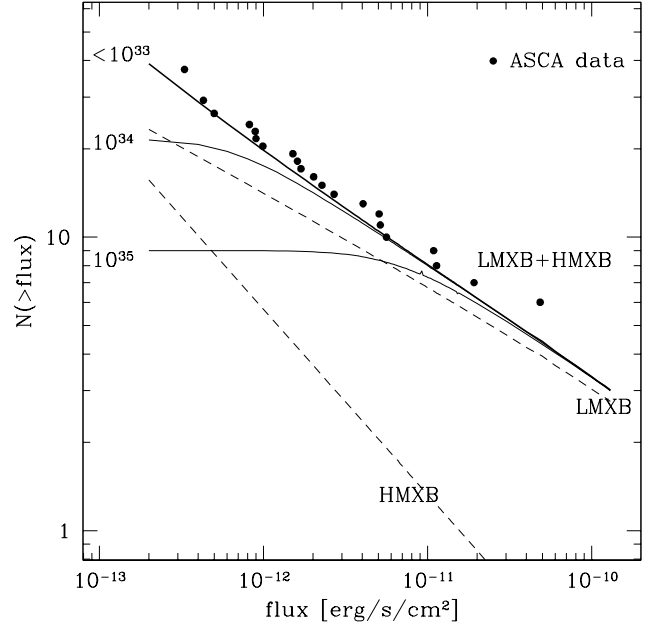


Fig. 18. Comparison of the number-flux relation observed in the ASCA Galactic Ridge Survey (points) and the predicted number–flux relation based on the extrapolation of the ASM luminosity function to low luminosities (lines). The vertical axis shows the number of sources in the entire field of the ASCA survey. The ASCA number–flux relation was corrected for the flux dependent sky coverage (Fig. 7 in Sugizaki et al. (2001)). The predicted number–flux relations were computed according to Eq. (17) using the extrapolation of the ASM luminosity functions and the volume density distributions of X-ray binaries described in Sect. 4. The thick solid lines show the combined $\text{Log}(N)\text{--}\text{Log}(S)$ of LMXBs and HMXBs for different values of the low luminosity cut-off. The thin dashed lines show the contributions of LMXBs and HMXBs separately for the case without cut-off.

The predicted $\text{Log}(N)\text{--}\text{Log}(S)$ calculated from Eq. (17) is compared with the $\text{Log}(N)\text{--}\text{Log}(S)$ of X-ray binary candidates from the ASCA survey in Fig. 18. In plotting the ASCA data (solid circles) we added five bright sources located in the ASCA field of view that were excluded from the final catalogue in Sugizaki et al. (2001) and corrected for the flux dependent sky coverage of the ASCA survey (Fig. 7 in Sugizaki et al. (2001)). The predicted $\text{Log}(N)\text{--}\text{Log}(S)$ was calculated according to Eq. (17) separately for HMXB and LMXB using the extrapolation of the respective ASM luminosity functions. The mass integral $M(< r)$ in Eq. (17) was calculated taking approximately into account the actual pattern of ASCA pointings and using the volume density distributions constructed in Sect. 4. The predicted combined $\text{Log}(N)\text{--}\text{Log}(S)$ of HMXB and LMXB sources is shown in Fig. 18 by the thick solid lines for different values of the low luminosity cut-off L_{\min} . The thin solid and dashed lines show the contributions of HMXBs

and LMXBs respectively for the case without low luminosity cut-off.

It is clear from Fig. 18 that the predicted number–flux relation of X-ray binaries agrees with the ASCA data very well. Given the volume density distributions of X-ray binaries in the Galaxy, the low flux end of the ASCA $\text{Log(N)}\text{--Log(S)}$ is sensitive to sources with luminosities of $\sim 10^{34} \text{ erg s}^{-1}$. The good agreement with the predicted $\text{Log(N)}\text{--Log(S)}$ distribution implies that the data do not require a low luminosity cut-off of the luminosity function down to $\sim 10^{34} \text{ erg s}^{-1}$.

7.3. Young objects in star forming regions

Recent observations with the CHANDRA X-ray observatory of the Orion Nebula cluster allow one to estimate the contribution to the X-ray emission from young objects in the star forming regions. Schulz et al. (2001) observed the Orion Trapezium region and found 111 sources above the sensitivity threshold of $6.6 \cdot 10^{28} \text{ erg s}^{-1}$, assuming a distance of 440 pc. The total luminosity of their sample is about $5.6 \cdot 10^{32} \text{ erg s}^{-1}$. This luminosity is dominated by the brightest source in the Orion Nebula cluster, $\theta^1 \text{ Ori C}$, which provides about $1.8 \cdot 10^{32} \text{ erg s}^{-1}$. Extrapolating this result to the whole Orion Nebula Cluster in which CHANDRA observed about 1000 sources we obtain a total luminosity of the star cluster of about $4 \cdot 10^{33} \text{ erg s}^{-1}$, counting the luminosity of $\theta^1 \text{ Ori C}$ only once and multiplying the rest by 10, assuming the luminosity function of the Trapezium region is representative for the whole Orion Nebula cluster. To estimate the X-ray luminosity of all star forming regions in the Galaxy one can proceed in two ways. Taking the mass of the molecular gas in the Orion cluster to be $\sim 10^5 M_\odot$ (Maddalena et al. 1986), and the total mass of the molecular gas in the Galaxy to be $\sim 10^9 M_\odot$ (Williams & McKee 1997), the total luminosity is $\sim 4 \cdot 10^{37} \text{ erg s}^{-1}$. On the other hand one can use the star formation rate in the Orion Nebula cluster and the Galaxy as the determining factor. Taking the SFR in Orion to be $\geq 10^{-4} M_\odot \text{ yr}^{-1}$ (Hillenbrand 1997), and the SFR in the Galaxy to be $4 M_\odot \text{ yr}^{-1}$ (McKee & Williams 1997), the total luminosity of young objects in the star forming regions in the Galaxy is $\lesssim 1.6 \cdot 10^{38} \text{ erg s}^{-1}$. Taking into account that the latter value is an upper limit, both numbers agree sufficiently well. Therefore star forming regions contribute less than \sim few per cent to the integrated X-ray emission of the Galaxy but $\sim 20\%$ or more to the luminosity of HMXBs in the energy range from 2–10 keV. On the other hand the spectrum of young stellar objects is much softer than the spectrum of X-ray binaries.

8. High luminosity sources

In recent months the CHANDRA X-ray observatory was able to resolve single X-ray sources in other galaxies that appear to radiate at or above the Eddington limit for a $1.4 M_\odot$ neutron star, i.e. $\sim 2 \cdot 10^{38} \text{ erg s}^{-1}$. Similar behaviour

is also observed in Galactic X-ray binaries by ASM. The slightly different spectral band used in these CHANDRA observations, usually 0.3–10 keV compared to 2–10 keV for ASM, does not lead to significant differences in luminosity.

Table 1 lists the sources which were observed either by ASM or some other instrument to emit at or above the Eddington limit for a $1.4 M_\odot$ neutron star. The spatial distribution of these sources is shown in Fig. 19 and can be compared to the distributions of the brightest sources observed by CHANDRA in other galaxies.

There are several reasons why sources can emit super-Eddington luminosity:

- For accreting black holes in high state radiation is coming from the quasi-flat accretion disk where electron scattering gives the main contribution to the opacity. Under these conditions the radiation is emitted according to

$$f(\mu) = (1 + 2.08\mu)\mu \quad (19)$$

where $\mu = \cos(i)$ where i is the inclination angle. It is easy to show that the radiation flux perpendicular to the plane of the disk exceeds the average value by 3 times (see Shakura & Sunyaev (1973) for discussion).

- Some of the normal stars entering the X-ray binary phase are strongly evolved and have an unusual chemical abundance, e.g. if a He-enriched star supplies matter the Eddington luminosity is twice higher than for hydrogen plasma due to the change in cross-section per nucleus.

Just these two factors permit to surpass the classical Eddington limit by a factor of ~ 6 .

- The star supplying material to the neutron star or black hole “does not know” about the existence of the Eddington luminosity limit due to accretion. Therefore some part of the matter will outflow forming a super-critical disk. In the approach of Shakura & Sunyaev (1973) it is possible to gain a factor of $\ln(\dot{m}) \approx 3\text{--}5$ for $\dot{m} \gg 1$ with $\dot{m} = \frac{\dot{M}}{M_{\text{Edd}}}$. Paczynsky & Wiita (1980) and Abramowicz et al. (1988) constructed the solution of slim disks which also permits luminosities higher than the Eddington luminosity.
- Many X-ray binaries show from time to time the acceleration of powerful jets (Mirabel & Rodríguez 1999). These relativistic jets might produce strongly beamed X-ray emission with flux strongly exceeding the average and Eddington critical value for isotropic sources. See also the discussion by Koerding et al. (2001), Fabrika & Mescheryakov (2000) and King et al. (2001).
- In the case of accretion on to a neutron star with strong magnetic field the accretion columns form near the surface of the neutron star in the polar regions. Such columns can have a super-Eddington luminosity, because photons are emitted perpendicular to the axis of the accretion column and the light pressure force is balanced by magnetic field (Basko & Sunyaev 1976).
- In Z-sources (luminous accreting neutron stars with low magnetic field) the boundary layer width expands

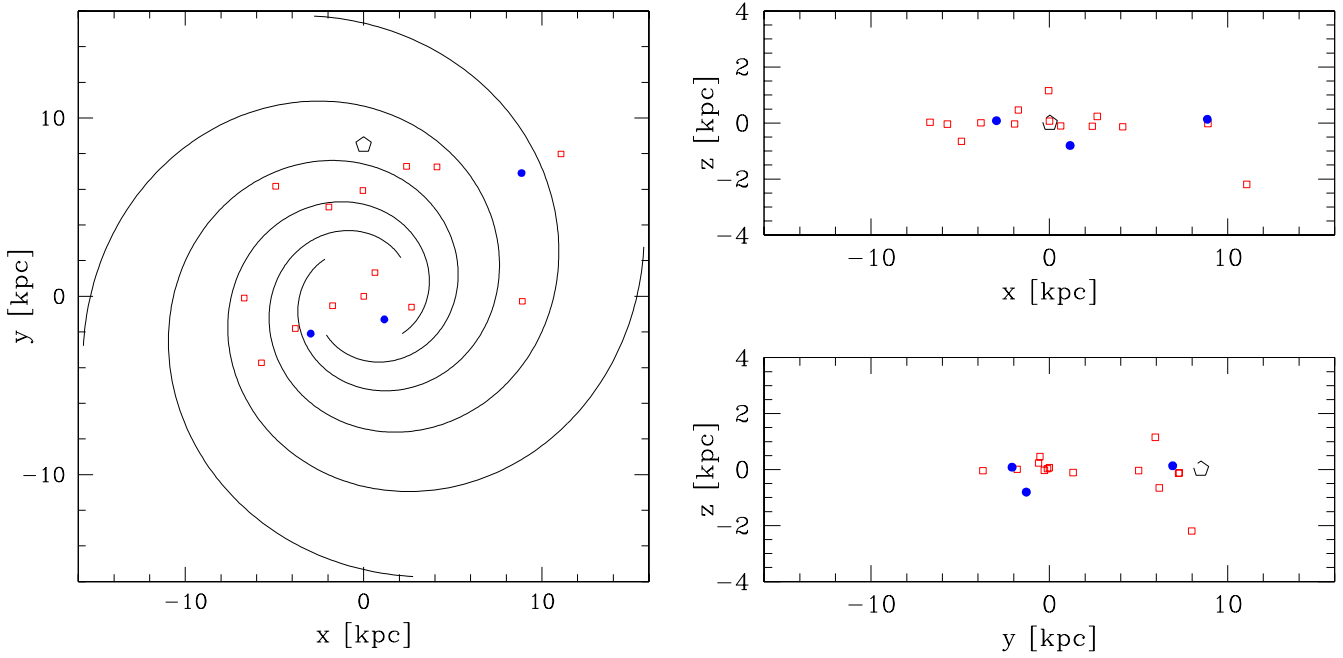


Fig. 19. The spatial distribution of Galactic X-ray binaries that have shown episodes of Eddington or super-Eddington luminosity for a $1.4 M_{\odot}$ neutron star. The coordinate system is the same as in Fig. 7. Filled circles indicate HMXBs, open squares indicate LMXBs. Note that fact that the majority of the sources are located at $y > 0$ reflects the flux limited nature of the ASM sample.

rapidly with increasing accretion rate reaching several star radii (Popham & Sunyaev 2001). This quasi-flat continuation of accretion disk might also have super-Eddington luminosity of the type of the slim disk.

9. Summary

We studied the population of X-ray binaries in the Milky Way.

- In good agreement with theoretical expectations and earlier results (van Paradijs & White 1995; White & van Paradijs 1996; Koyama et al. 1990; Nagase 1989) we found significant differences in the spatial (3-D) distribution of high and low mass X-ray binaries. HMXBs are more concentrated towards the Galactic Plane with a vertical scale height of 150 pc, tend to avoid the Galactic Bulge and central $\sim 3 - 4$ kpc of the Galaxy and show clear signatures of the spiral structure. The distribution of LMXB sources, on the contrary, peaks strongly at the Galactic Bulge and shows a pronounced minimum at $\sim 3 - 4$ kpc. Some signatures of the Galactic spiral structure are also present. The vertical distribution of LMXB sources is significantly broader, with a scale height of 410 pc.
- We constructed the *long-term averaged* Log(N)–Log(S) distribution of high and low mass X-ray binaries in the 2–10 keV energy range using the data of the ASM instrument aboard RXTE from 1996–2000 to the limiting sensitivity of $\approx 6.4 \cdot 10^{-11} \text{ erg s}^{-1} \text{ cm}^{-2}$. The Log(N)–Log(S) distribution of HMXBs is

well described by a simple power law with a slope of the differential distribution of $1.61_{-0.14}^{+0.12}$ down to a flux limit of $\approx 6.4 \cdot 10^{-11} \text{ erg s}^{-1} \text{ cm}^{-2}$. The differential Log(N)–Log(S) distribution of LMXBs has a slope of -1.2 ± 0.06 and requires a high-flux cutoff at $\sim 110 \text{ ASM cnts s}^{-1}$, $\approx 3.5 \cdot 10^{-8} \text{ erg s}^{-1} \text{ cm}^{-2}$. A comparison with data of the ASCA Galactic Ridge Survey (Sugizaki et al. 2001) which covered ~ 40 square degrees with ~ 100 times better sensitivity did not reveal any evidence of significant departures of the Log(N)–Log(S) from an extrapolation of the ASM data down to $\approx 5 \cdot 10^{-13} \text{ erg s}^{-1} \text{ cm}^{-2}$.

- Using the source distances available and assuming a model for the volume density distribution we constructed luminosity functions for HMXBs and LMXBs in the 2–10 keV energy range. The sensitivity limit of the ASM catalogue allows one to study the XRB luminosity functions down to a luminosity of $\sim 2 \cdot 10^{35} \text{ erg s}^{-1}$. The differential luminosity functions can be described by a power law with slopes of 1.64 and 1.27 for HMXBs and LMXBs respectively. For LMXB sources a cut-off at $\sim 2.7 \cdot 10^{38} \text{ erg s}^{-1}$ is required. The HMXB data are insufficient to detect a high luminosity cut-off above $\sim \text{few} \times 10^{36} \text{ erg s}^{-1}$. A comparison with the data of ASCA Galactic Ridge Survey did not find evidence for significant departures from these power laws down to luminosities of $\sim 10^{34} \text{ erg s}^{-1}$.
- The complete catalogue of our sample of X-ray binaries is available at <http://www.mpa->

- garching.mpg.de/~grimm/. Properties of the brightest sources are summarised in Tables 5, 6, 1.
- The integrated luminosity of X-ray binaries in the Milky Way in the 2–10 keV band averaged over 1996–2000 is $\sim 2 - 3 \cdot 10^{39}$ erg s $^{-1}$ to which LMXB sources contribute $\sim 90\%$. Normalised to the stellar mass and the star formation rate the integrated luminosity of LMXBs ($\sim 2.5 \cdot 10^{39}$ erg s $^{-1}$) and HMXBs ($\sim 2 \cdot 10^{38}$ erg s $^{-1}$) correspond to $\sim 5 \cdot 10^{28}$ erg s $^{-1}$ M $_{\odot}^{-1}$ and $\sim 5 \cdot 10^{37}$ erg s $^{-1}$ /(M $_{\odot}$ yr $^{-1}$), respectively. The total number of the X-ray binaries brighter than $2 \cdot 10^{35}$ erg s $^{-1}$ is ~ 190 of which ~ 55 are high mass and ~ 135 are low mass binaries. Extrapolating the luminosity functions towards low luminosities we estimate the total number of the X-ray binaries brighter than 10^{34} erg s $^{-1}$ as ~ 705 (~ 325 LMXB and ~ 380 HMXB sources). These estimates might be subject to the uncertainty of a factor of ~ 2 due to insufficient knowledge of the spatial distribution of X-ray binaries in the Galaxy.
 - Due to the shallow slope of the luminosity function the integrated X-ray emission of the Milky Way is dominated by $\sim 5 - 10$ brightest sources. Variability of individual sources or an outburst of a bright transient source can increase the integrated luminosity of the Milky Way by as much as a factor of ~ 2 .
 - We found that at least 16 sources in the Galaxy showed episodes of super-Eddington luminosity for a 1.4 M $_{\odot}$ neutron star. We plotted the distribution of these sources across the Galaxy in various projections, which can be used to compare with the recent CHANDRA and XMM-Newton images of the nearby galaxies.
- ### acknowledgements
- This research has made use of data and results provided by the ASM/RXTE teams at MIT and at the RXTE SOF and GOF at NASAs GSFC. Data were obtained through the High Energy Astrophysics Science Archive Research Center Online Service, provided by the NASA/Goddard Space Flight Center. We also want to thank the referee for helpful remarks on the paper.
- ### References
- Abramowicz, M., Czerny, B., Lasota, J., & Szuszkiewicz, E. 1988, *ApJ*, 332, 646
- Angelini, L., Loewenstein, M., & Mushotzky, R. F. 2001, *ApJ*, 557, L35
- Bahcall, J. 1978, in *Proceedings of the International School of Physics "Enrico Fermi"*, Vol. 65, Physics and astrophysics of neutron stars and black holes, ed. R. Giacconi & R. Ruffini (Italian Phys. Soc.), 63
- Bahcall, J. N. & Soneira, R. M. 1980, *ApJS*, 44, 73
- Bandyopadhyay, R. M., Shahbaz, T., Charles, P. A., & Naylor, T. 1999, *MNRAS*, 306, 417
- Barret, D., McClintock, J. E., & Grindlay, J. E. 1996, *ApJ*, 473, 963
- Barret, D., Motch, C., & Predehl, P. 1998, *A&A*, 329, 965
- Basko, M. M. & Sunyaev, R. A. 1976, *MNRAS*, 175, 395
- Binney, J., Gerhard, O., & Spergel, D. 1997, *MNRAS*, 288, 365
- Blanton, E. L., Sarazin, C. L., & Irwin, J. A. 2001, *ApJ*, 552, 106
- Bradshaw, C. F., Fomalont, E. B., & Geldzahler, B. J. 1999, *ApJ*, 512, L121
- Brandt, H., Rotschild, R., & Swank, J. 1996, in *Memorie della Societa Astronomica Italiana*, Vol. 67, 593
- Bridges, T. J. & Hanes, D. A. 1990, *AJ*, 99, 1100
- Chakrabarty, D., Grunsfeld, J. M., Prince, T. A., et al. 1993, *ApJ*, 403, L33
- Chevalier, C. & Ilovaisky, S. A. 1990, *A&A*, 238, 163
- Christian, D. J. & Swank, J. H. 1997, *ApJS*, 109, 177
- Corbet, R. H. D., Marshall, F. E., Peele, A. G., & Takeshima, T. 1999, *ApJ*, 517, 956
- Cowley, A. P., Crampton, D., & Hutchings, J. B. 1979, *ApJ*, 231, 539
- Dehnen, W. & Binney, J. 1998, *MNRAS*, 294, 429
- Di Stefano, R., Kong, A. K. H., Garcia, M. R., et al. 2002, *ApJ*, 570, 618
- Djorgovski, S. 1993, in *ASP Conf. Ser. 50: Structure and Dynamics of Globular Clusters*, 373
- Downes, D., Wilson, T. L., Biegging, J., & Wink, J. 1980, *A&AS*, 40, 379
- Dwek, E., Arendt, R., Hauser, M., et al. 1995, *ApJ*, 445, 716
- Ebisuzaki, T., Sugimoto, D., & Hanawa, T. 1984, *PASJ*, 36, 551
- Englmaier, P. & Gerhard, O. 1999, *MNRAS*, 304, 512
- Fabbiano, G., Zezas, A., & Murray, S. 2001, *ApJ*, 554, 1035
- Fabrika, S. & Mescheryakov, A. 2000, in *IAU Symposium*, Vol. 205, E105
- Fender, R. P. 2001, *MNRAS*, 322, 31
- Finoguenov, A. & Jones, C. 2001, *ApJL*, 547, 107
- Forman, W., Jones, C., Cominsky, L., et al. 1978, *ApJS*, 38, 357
- Garcia, M. R., Murray, S. S., Primini, F. A., Forman, W. R., & Jones, C. 2000, in *IAU Symposium*, Vol. 205
- Georgelin, Y. & Georgelin, Y. 1976, *A&A*, 49, 57
- Grebenev, S. A., Pavlinsky, M. N., & Sunyaev, R. 1996, in *Röntgenstrahlung from the Universe*, 141
- Greiner, J., Cuby, J., McCaughrean, M., Castro-Tirado, A., & Mennickent, R. 2001, submitted to *A&A*
- Greiner, J., Hasinger, G., Molendi, S., & Ebisawa, K. 1994, *A&A*, 285, 509
- Griffiths, R., Ptak, A., Feigelson, E., et al. 2000, *Science*, 290, 1325
- Haberl, F. & Titarchuk, L. 1995, *A&A*, 299, 414
- Harris, W. E. & Racine, R. 1979, *ARA&A*, 17, 241
- Hillenbrand, L. A. 1997, *AJ*, 113, 1733
- Hutchings, J. B., Cowley, A. P., Crampton, D., van Paradijs, J., & White, N. E. 1979, *ApJ*, 229, 1079
- Illarionov, A. & Sunyaev, R. 1975, *A&A*, 39, 185
- Israel, G., Negueruela, I., Campana, S., et al. 2001, *A&A*, 371, 1018

- Kaper, L., Lamers, H. J. G. L. M., Ruymaekers, E., van den Heuvel, E. P. J., & Zuidervijk, E. J. 1995, *A&A*, 300, 446
- King, A., Davies, M., Ward, M., Fabbiano, G., & Elvis, M. 2001, *ApJ*, 552, L109
- King, A. R. 1993, *MNRAS*, 260, L5
- Kitamoto, S., Tsunemi, H., Miyamoto, S., & Hayashida, K. 1992, *ApJ*, 394, 609
- Koerding, E., Falcke, H., Markoff, S., & Fender, R. 2001, in *Astronomische Gesellschaft Meeting Abstracts*, Vol. 18, 176
- Koyama, K., Kawada, M., Kunieda, H., Tawara, Y., & Takeuchi, Y. 1990, *Nature*, 343, 148
- Krzeminski, W. 1974, *ApJ*, 192, L135
- Kuijken, K. & Rich, R. M. 2001, in *American Astronomical Society Meeting*, Vol. 199, 9113
- Lamb, R. C., Markert, T. H., Hartman, R. C., Thompson, D. J., & Bignami, G. F. 1980, *ApJ*, 239, 651
- Levine, A. M., Bradt, H., Cui, W., et al. 1996, *ApJ*, 469, L33
- Liu, Q. Z., van Paradijs, J., & van den Heuvel, E. P. J. 2000, *A&AS*, 147, 25
- . 2001, *A&A*, 368, 1021
- Lochner, J. & Remillard, R. 1997, *The XTE All Sky Monitor Data Products*, http://heasarc.gsfc.nasa.gov/docs/xte/asm_products_guide.html
- Maddalena, R., Morris, M., Moscowitz, J., & Thaddeus, P. 1986, *ApJ*, 303, 375
- Makishima, K., Hayashida, K., Inoue, H., et al. 1989, *PASJ*, 41, 697
- Markert, T., Winkler, P., Laird, F., et al. 1979, *ApJS*, 39, 573
- Martin, A. C., Casares, J., Charles, P. A., van der Hooft, F., & van Paradijs, J. 1995, *MNRAS*, 274, L46
- Massey, P., Johnson, K. E., & Degioia-Eastwood, K. 1995, *ApJ*, 454, 151
- Matilsky, T., Gursky, H., Kellogg, E., et al. 1973, *ApJ*, 181, 753
- McKee, C. F. & Williams, J. P. 1997, *ApJ*, 476, 144
- Mirabel, I. & Rodríguez, L. 1994, *Nature*, 371, 46
- Mirabel, I. & Rodríguez, L. 1999, *ARA&A*, 37, 409
- Motch, C., Haberl, F., Dennerl, K., Pakull, M., & Janot-Pacheco, E. 1997, *A&A*, 323, 853
- Murdoch, H. S. & Crawford, D. F. 1973, *ApJ*, 183, 1
- Nagase, F. 1989, in *Two Topics in X-Ray Astronomy*, Volume 1: X Ray Binaries. Volume 2: AGN and the X Ray Background, 45–55
- Nakamura, N., Dotani, T., Inoue, H., et al. 1989, *PASJ*, 41, 617
- Narayan, R. & Yi, I. 1995, *ApJ*, 452, 710
- Neff, S. G. & Ulvestad, J. S. 2000, *AJ*, 120, 670
- Nishiuchi, M., Koyama, K., Maeda, Y., et al. 1999, *ApJ*, 517, 436
- Ogasaka, Y., Kii, T., Ueda, Y., et al. 1998, *AN*, 319, 43
- Orosz, J. A., Bailyn, C. D., McClintock, J. E., & Remillard, R. A. 1996, *ApJ*, 468, 380
- Orosz, J. A., Groot, P. J., van der Klis, M., et al. 2002, *ApJ*, 568, 845
- Orosz, J. A. & Kuulkers, E. 1999, *MNRAS*, 305, 132
- Orosz, J. A., Kuulkers, E., van der Klis, M., et al. 2000, in *American Astronomical Society Meeting*, Vol. 197, 8320
- Paczynsky, B. & Wiita, P. 1980, *A&A*, 88, 23
- Penninx, W. 1989, in *X-ray astronomy*, ed. J. Hunt & B. Battrick, *Proceedings of the 23rd ESLAB Symposium No. ESA SP-296 (ESA)*, 185
- Piccinotti, G., Mushotzky, R., Boldt, E., et al. 1982, *ApJ*, 253, 485
- Popham, R. & Sunyaev, R. 2001, *ApJ*, 547, 355
- Predehl, P., Burwitz, V., Paerels, F., & Trümper, J. 2000, *A&A*, 357, L25
- Reynolds, A. P., Bell, S. A., & Hilditch, R. W. 1992, *MNRAS*, 256, 631
- Ritter, H. & Kolb, U. 1998, *A&AS*, 129, 83
- Sarazin, C., Irwin, J., & Bregman, J. 2000, *ApJ*, 544, L101
- Sazonov, S. Y., Sunyaev, R. A., & Lund, N. 1997, *Pis ma Astronomicheskii Zhurnal*, 23, 326
- Schulz, N., Canizares, C., Huenemoerder, D., et al. 2001, *ApJ*, 549, 441
- Shakura, N. & Sunyaev, R. 1973, *A&A*, 24, 337
- Shirey, R., Soria, R., Borozdin, K., et al. 2001, *A&A*, 365, L195
- Simonson, S. C. 1976, *A&A*, 46, 261
- Smale, A. P. 1998, *ApJ*, 498, L141
- Smith, D. A., Morgan, E. H., & Bradt, H. 1997, *ApJ*, 479, L137
- Smith, D. S. & Wilson, A. S. 2001, *ApJ*, 557, 180
- Solomon, P., Sanders, D., & Rivolo, A. 1985, *ApJL*, 292, 19
- Sugizaki, M., Mitsude, K., Kaneda, H., et al. 2001, *ApJS*, 134, 77
- Sunyaev, R. 1990, *IAUC*, 5104, 1
- Sunyaev, R. & Revnivtsev, M. 2000, *A&A*, 358, 617
- Tanaka, Y. 1992, in *X-ray binaries and recycled pulsars*, ed. E. van den Heuvel & S. Rappaport, Vol. C 377 (Kluwer), 37
- Taylor, J. & Cordes, J. 1993, *ApJ*, 411, 674
- Tennant, A. F., Wu, K., Ghosh, K. K., Kolodziejczak, J. J., & Swartz, D. A. 2001, *ApJ*, 549, L43
- Tsunemi, H., Kitamoto, S., Okamura, S., & Roussel-Dupre, D. 1989, *ApJ*, 337, L81
- Vallée, J. 1995, *ApJ*, 454, 119
- van Paradijs, J. 1994, *Cambridge Astrophysics Series*, Vol. 26, *X-ray binaries* (Cambridge University Press), 536
- van Paradijs, J. & White, N. 1995, *ApJ*, 447, L33
- Verbunt, F. 1996, in *NATO ASIC Proc. 477: Evolutionary Processes in Binary Stars*, 201
- Wachter, S. & Margon, B. 1996, *AJ*, 112, 2684
- Warwick, R., Marshall, N., Fraser, G., et al. 1981, *MNRAS*, 197, 865
- Watson, M. G., Ricketts, M. J., & Griffiths, R. E. 1978, *ApJ*, 221, L69
- Webbink, R. F. 1985, in *IAU Symp. 113: Dynamics of Star Clusters*, Vol. 113, 541

- Wen, L., Remillard, R. A., & Bradt, H. V. 2000, *ApJ*, 532, 1119
- White, N., Kaluzienski, J., & Swank, J. 1984, in *High Energy Transients in Astrophysics*, ed. S. Woosley, AIP Conference Proceedings No. 115 (New York: American Institute of Physics), 31–48
- White, N. E., Becker, R. H., Pravdo, S. H., et al. 1980, *ApJ*, 239, 655
- White, N. E. & van Paradijs, J. 1996, *ApJ*, 473, L25
- Williams, J. P. & McKee, C. F. 1997, *ApJ*, 476, 166
- Zezas, A., Fabbiano, G., Ward, M., Prestwich, A., & Murray, S. 2001, in *American Astronomical Society Meeting*, Vol. 198, 5011
- Zombeck, M. V. 1990, *Handbook of Space Astronomy and Astrophysics*, 2nd edn. (Cambridge University Press)